WIRELESS IN-BODY SENSING AND ACTUATION THROUGH GENETICALLY MODIFIED BACTERIA

by

Ahmet Bilir

B.S., Electrical and Electronics Enginneering, Boğaziçi University, 2023

Submitted to the Institute for Graduate Studies in
Science and Engineering in partial fulfillment of
the requirements for the degree of
Master of Science

Graduate Program in Electrical and Electronics Enginneering
Boğaziçi University

2025

WIRELESS IN-BODY SENSING AND ACTUATION THROUGH GENETICALLY MODIFIED BACTERIA

APPROVED BY:

Assoc. Prof. Sema Dumanli Oktar (Thesis Supervisor)	.....
Prof. Arda Deniz Yalcinkaya	.....
Assoc. Prof. Urartu Ozgur Safak Seker	.....

DATE OF APPROVAL: 19.09.2025

ACKNOWLEDGEMENTS

First and foremost, I would like to express my deepest gratitude to my thesis advisor, Assoc. Prof. Sema Dumanlı Oktar. This work would not have been possible without her unwavering support, invaluable guidance, and endless patience throughout every stage of this journey.

I would also like to thank the jury members, Prof. Dr. Arda Deniz Yalcinkaya and Assoc. Prof. Urartu Ozgur Safak Seker.

I would also like to extend my sincere thanks to all members of the BOUN-TENNA research group for creating such a collaborative and inspiring environment. In particular, I am especially grateful to Burak Ferhat Ozcan, Anil Tulu, Mehmet Emre Korkmaz, Ipek Kacar, Cagla Karabulut, Ozan Furkan Sezgen and Oguz Kaan Erden for their invaluable collaboration and shared efforts throughout this journey.

I am also thankful to Assoc. Prof. Urartu Ozgur Safak Seker and Dr. Merve Yavuz for providing the genetically engineered bacteria used in this study and for their guidance throughout the process. I am grateful to Assist. Prof. Cansu Canbek for granting me access to the fluorometer and spectrophotometer, and to Aleyna Isler and Elif Sumeyye Cirit for their assistance during the measurements.

Last but not least, I would like to thank my family for their unconditional support.

Part of the text was edited using ChatGPT (OpenAI), and some figures were created or edited using BioRender.

This work was supported by the Scientific and Technological Research Council of Turkey (TUBITAK) under Grant No. 120C131.

ABSTRACT

WIRELESS IN-BODY SENSING AND ACTUATION THROUGH GENETICALLY MODIFIED BACTERIA

This thesis introduces a new class of fully passive, wireless bio-hybrid implants that integrate genetically engineered bacteria with microwave resonators to enable molecular-level sensing and wireless control inside the body. Synthetic biology offers powerful tools to reprogram living cells for detecting specific target molecules; however, the lack of viable wireless communication mechanisms has limited their use in vivo. Direct electromagnetic interaction with individual cells would require THz frequencies, which are strongly attenuated in biological tissues. To overcome this, this work links cellular responses to electromagnetic signals by coupling engineered *E. coli* with a biodegradable passive microwave antenna. The bacteria modulate the antenna's degradation rate, and the resulting resonance shifts are wirelessly tracked using backscatter communication. This approach enables real-time, battery-free molecular sensing at an implant depth of 25 mm in muscle-mimicking phantoms.

In addition, this thesis demonstrates a method for wireless thermal actuation of engineered bacteria using focused microwave hyperthermia. An on-body antenna delivers energy to the implanted resonator, producing localized heating while maintaining the temperature of surrounding tissue below the 43°C safety threshold. Multiphysics simulations show that the system can induce a localized temperature rise exceeding 6°C within 5 minutes under 1 W input power—sufficient to activate heat-inducible genetic circuits and trigger protein expression. This work represents the first demonstration of a wireless link between a passive, cell-based implant and an on-body antenna, laying the groundwork for battery-free, circuit-free cellular implants for continuous biosensing and programmable therapeutic applications.

ÖZET

GENETİĞİ DEĞİŞTİRİLMİŞ BAKTERİLERLE KABLOSUZ BEDEN İÇİ ALGILAMA VE UYARIM

Bu tez, genetiği değiştirilmiş bakterileri mikrodalga rezonatörlerle entegre eden, tamamen pasif ve kablosuz çalışan yeni bir biyo-hibrit implant sınıfı sunmaktadır. Sistem, beden içerisinde moleküler düzeyde algılama ve kablosuz kontrol imkânı sağlamaktadır. Sentetik biyoloji, hücreleri belirli molekülleri algılayacak şekilde yeniden programlamaya olanak verse de, uygun kablosuz iletişim mekanizmalarının eksikliği bu sensörlerin in vivo kullanımını sınırlamaktadır. Hücrelerle doğrudan elektromanyetik etkileşim sağlamak, biyolojik dokularda şiddetle zayıflayan THz frekanslarını gerektirir. Bu sınırlamayı aşmak için bu çalışmada, genetiği değiştirilmiş bakteri biyobozunur pasif bir antenle birleştirilmiş ve bakterilerin tepkisi antenin bozunma hızını değiştirecek şekilde tasarlanmıştır. Antenin bozunma hızının modüle edilmesiyle antenin rezonans frekansı değişmekte, bu değişim gerisaçılım (backscatter) yöntemiyle kablosuz olarak izlenmektedir. Bu yaklaşımla bataryasız ve elektronik komponent içermeyen implantlarla beden-içi gerçek zamanlı moleküler algılamanın mümkün olduğu gösterilmiştir.

Ayrıca bu tezde, mikrodalga hipertermi kullanılarak genetiği değiştirilmiş bakterilerin kablosuz termal uyarımına yönelik bir yöntem geliştirilmiştir. Beden yüzeyine yerleştirilen bir anten, implant rezonatörde lokal sıcaklık artışı oluştururken çevre dokunun sıcaklığını 43°C eşiğinin altında tutmaktadır. Multifizik benzetimler, sistemin 1 W güç altında 5 dakikada 6°C'den fazla sıcaklık artışı sağladığını göstermiştir. Bu düzeydeki sıcaklık artışı, ısı ile uyarılabilir genetik devreleri aktive ederek protein üretimini tetiklemektedir. Bu çalışma, pasif ve hücre tabanlı bir implant ile beden-üstü okuyucu arasında kablosuz bağlantı kurulan ilk örneği temsil etmekte ve pil ya da devre gerektirmeyen hücresel implantların geliştirilmesine temel oluşturmaktadır.

TABLE OF CONTENTS

LIST OF FIGURES

LIST OF SYMBOLS

J	Joule
K	Kelvin
kg	kilogram
mm	millimeter
nm	nanometer
S/m	Siemens per meter
S_{11}	Reflection Coefficient
S_{21}	Transmission Coefficient
W	Watt
ϵ_r	Relative Permittivity
σ	Conductivity
°C	degree Celcius

LIST OF ACRONYMS/ABBREVIATIONS

2D	Two Dimensional
3D	Three Dimensional
ABS	Acrylonitrile–Butadiene–Styrene
AMP	Ampicillin
CCM	Cytochrome C Maturation
CMR	Chloramphenicol
CNN	Convolutional Neural Network
CymA	Cytochrome c-type Membrane Protein A
DAK	Dielectric Assessment Kit
dB	Decibel
DPV	Differential Pulse Voltammetry
ECM	Extracellular Matrix
EET	Extracellular Electron Transfer
EM	Electromagnetic
GHz	Gigahertz
HFSS	High Frequency Structure Simulator
HSR	Heat Shock Response
LB	Luria–Bertani
MOPS	3-(N-morpholino)Propanesulfonic Acid
mtr	Metal Reduction
NAND	Not And
NapC	Nitrate Reductase System Protein C
NOR	Not Or
OD	Optical Density
PBS	Phosphate-buffered Saline
PCB	Printed Circuit Board
PDMS	Polydimethylsiloxane
PET	Polyethylene Terephthalate

PF4	Porous Foam type 4
RFID	Radio Frequency Identification
RNA	Ribonucleic Acid
SAR	Specific Absorption Rate
sfGFP	Superfolder Green Fluorescent Protein
SLA	Stereolithography
SRR	Split-ring Resonator
VNA	Vector Network Analyzer
WCS	Whole-cell Sensors
WPT	Wireless Power Transfer
XOR	Exclusive Or

1. INTRODUCTION

Recent advances in biomedical engineering are increasingly blurring the boundaries between living systems and electronic devices. Conventional implantable medical devices—such as pacemakers, glucose monitors, and neurostimulators—have already transformed healthcare by enabling continuous monitoring and intervention inside the human body. However, these devices remain constrained by their reliance on rigid materials, batteries, and complex electronics, which limit their long-term biocompatibility, miniaturization, and functionality. At the same time, synthetic biology has opened new possibilities to program living cells with user-defined sensing and actuation functions. Integrating these programmable biological components with wireless passive electronics offers a promising path toward a new class of bio-hybrid implants that operate without internal power sources or circuitry. This thesis explores this concept by developing a system that combines genetically engineered bacteria with an implant antenna to achieve two key capabilities: (i) wireless molecular sensing and (ii) wireless thermal actuation.

1.1. Wireless Molecular Sensing

The global population is steadily increasing, with a particularly rapid rise in the proportion of elderly individuals. This demographic trend is expected to place an unprecedented burden on healthcare systems worldwide. Current healthcare infrastructures are unlikely to meet the growing demand without fundamental change. Addressing this challenge requires a paradigm shift in how healthcare is delivered—extending beyond hospitals and home-based care to include new ways of continuously monitoring human health. In this context, implantable sensors capable of tracking physiological conditions and enabling early diagnosis—before the onset of symptoms—represent a critical step toward the future of healthcare [1–3].

A wide range of implantable devices has been reported in the literature for various monitoring, diagnostic, and therapeutic purposes [4,5]. These devices typically monitor physical or physiological parameters, such as in capsule endoscopy [6], brain–computer interfaces [7], glucose sensing [8, 9], pH measurement [10], and intravascular pressure monitoring [11]. For example, the electromagnetic wave–based glucose detection system described in [12] estimates glucose concentration indirectly by observing changes in tissue permittivity. Such approaches do not achieve molecule-specific detection, which is essential for early and precise diagnosis. Present passive implantable sensor technologies are therefore limited in their ability to detect specific biomarkers in vivo and in real time [13].

One strategy to overcome this limitation is to incorporate engineered living cells as sensing elements. Biological systems are naturally equipped with highly specific molecular recognition mechanisms, and synthetic biology provides tools to reprogram living cells to act as specialized biosensors [14, 15]. Whole-cell molecular sensors could open new possibilities for highly sensitive and specific diagnostics [16]. While electrochemical or nanotechnology-based biosensors capable of molecular detection have been demonstrated [17–19], these are generally restricted to in vitro settings and cannot provide continuous in vivo measurements. Recent studies have begun to address this gap by developing platforms for real-time molecular sensing within living organisms. For example, Saunders et al. proposed aptamer- and antibody-based molecular switches for continuous detection using optical readouts via fiber-optic interfaces [20]. Chen et al. developed an optical system for in vivo molecular sensing in the blood vessels of freely moving rats [21], and Moutsiopoulou et al. explored aptamer-based optical techniques [22]. Other studies, such as those by Chien et al. and Chen et al., have introduced wireless and inductively coupled aptamer-based sensors [23, 24]. However, these systems still depend on integrated electronics, batteries, or optical fibers, which complicate long-term implantation and limit their applicability.

To move beyond these limitations, this thesis investigates a bio-hybrid sensing concept that integrates genetically engineered bacteria with a biodegradable passive im-

plant antenna. Unlike conventional sensors, this system is designed to operate without batteries or embedded electronics. The core idea is to link molecular-level biological responses to wireless electromagnetic signals. Synthetic biology allows living cells—such as *E. coli*—to be engineered to respond to specific molecules [25–29]. The challenge then becomes translating these cellular responses into measurable signals that can be acquired wirelessly. This thesis explores such an interface, which enables passive wireless monitoring.

In this approach, a bio-hybrid implant consisting of a magnesium antenna and genetically modified *E.coli* is wirelessly coupled to an external on-body reader antenna. The implant antenna is designed to undergo controlled biodegradation, which shifts its resonant frequency over time. This frequency shift can be tracked wirelessly using backscatter communication. By programming the bacteria to accelerate magnesium degradation in the presence of a target molecule, the system can report molecular activity indirectly through changes in the wireless response. Similar biodegradable wireless implants have been proposed in previous studies [30, 31]. In this work, two scenarios are examined: *E.coli* with and without the synthetic genetic circuit responsible for accelerating magnesium degradation. While the specific molecule that triggers this response is beyond the scope of this thesis, the focus is on demonstrating the feasibility of establishing a wireless communication link mediated by genetically engineered bacteria.

Understanding how genetic modifications influence the interaction between living cells and conductive materials is essential for this concept. Electroactive bacteria naturally perform extracellular electron transfer (EET), using redox-active proteins to exchange electrons with external acceptors such as metals or metal oxides [32–34]. Species such as Geobacter and Shewanella exemplify this process, transferring electrons along conductive nanowires to distant minerals during anaerobic respiration. Such mechanisms demonstrate how living cells can affect the electrical properties of their surroundings. Synthetic biology enables similar capabilities in non-electroactive species by heterologously expressing c-type cytochrome proteins—particularly those

in the MtrCAB pathway, which requires cytochrome c maturation (Ccm) proteins for functionality [36–41]. This thesis aims to equip *E.coli* with EET capability, creating bioelectrochemical sentinel cells capable of modulating material properties and enabling molecular-level sensing. Such bio-hybrid sensors could enable real-time monitoring of physiological processes and early detection of disease biomarkers, opening a new direction for implantable medical devices.

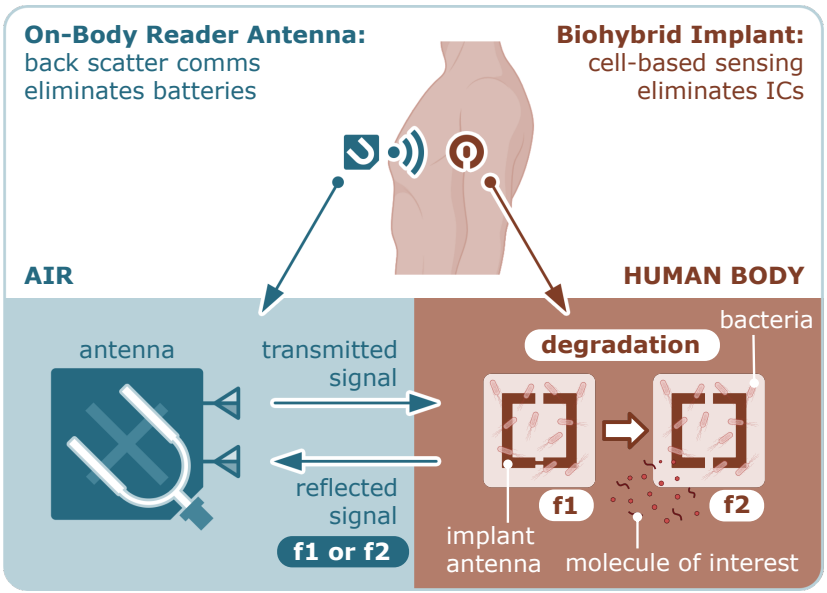

Figure 1.1. The AntennAlive concept illustrating the principle of operation for genetically modified bacteria-based wireless sensing [35]. The illustration of the implant antenna was created in BioRender.com.

1.2. Wireless Actuation

Implantable electronic systems have undergone significant advancements over the past decade, enabling continuous in vivo sensing and actuation through wireless links to external systems. Most of these systems, however, follow a conventional design paradigm composed of discrete sensing, processing, power, and communication modules. Such architectures present challenges for long-term implantation due to their size, power requirements, and the potential cytotoxic effects of their materials. Biocompatibility is generally achieved through the use of inert encapsulation layers, which

only offer partial and temporary protection against immune responses [42]. These constraints limit the practicality of conventional electronic implants, especially in chronic implantation scenarios.

To address these limitations, previous studies have introduced an alternative approach that employs genetically engineered living cells as the primary sensing elements [35]. Building on earlier work involving bio-hybrid implants capable of molecular-scale sensing [16], [43], the present thesis explores the integration of wireless downlink functionality within such architectures. The proposed system consists of a bio-hybrid implant incorporating genetically modified *E. coli* alongside a passive microwave resonator. Wireless actuation is achieved using an external on-body antenna, eliminating the need for batteries or embedded electronic circuits within the implant. The broader objective is to enable the wireless control of cellular behavior inside the body, thereby creating programmable biological responses on demand. Such wireless modulation of bacterial activity could be applied to therapeutic tasks such as targeted drug delivery; for example, engineered *E.coli* could be programmed to produce glucagon-like peptide-1 to reduce insulin dependency in diabetic patients.

Although synthetic biology provides powerful tools for programming cellular behavior, current methods for wirelessly controlling cells face critical limitations in terms of penetration depth. Establishing a direct electromagnetic interface with individual cells inside the body is fundamentally restricted by scale: interaction at the cellular level would require electromagnetic wavelengths comparable to cellular dimensions, implying operation at terahertz frequencies and beyond [44]. However, biological tissues exhibit very high dielectric losses at such frequencies. At 1 GHz, human tissue permittivity ranges between 3.5 and 68, with conductivities up to 2.5 S/m [45]. This results in severe attenuation, making direct high-frequency in-body communication infeasible. In practice, in-body communication is limited to sub-6 GHz microwave frequencies, which do not provide the spatial resolution necessary for cell-level interaction. To overcome this challenge, the system proposed in this thesis employs thermally triggered biological responses rather than direct electromagnetic stimulation of cells.

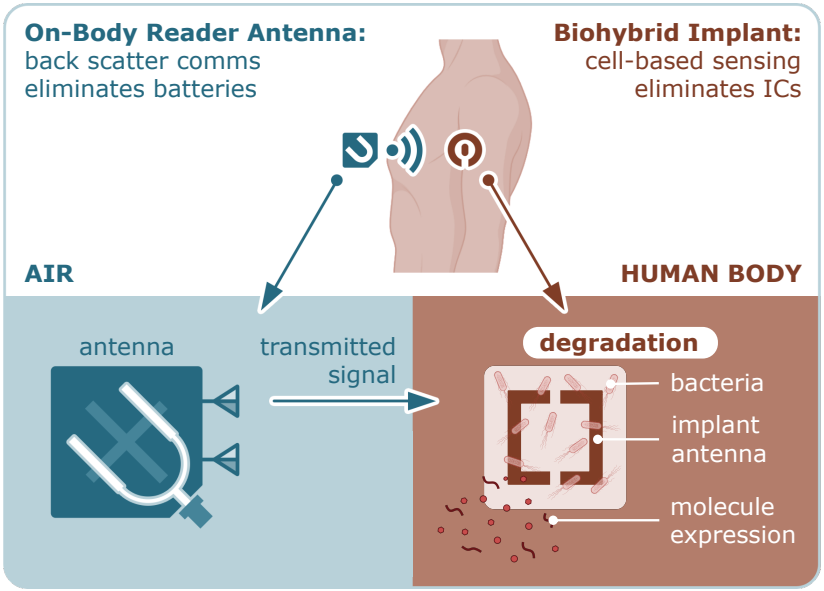

Figure 1.2. The concept of the wireless actuation of the genetically engineered bacteria. The illustration of the implant antenna was created in BioRender.com.

Thermal modulation has been used in biomedical applications. Conventional thermal therapies generally target macroscopic tissue regions [46]. Various implementations of non-invasive microwave hyperthermia have been reported, all aiming to focus electromagnetic energy on a defined region while minimizing collateral heating of healthy tissue [47]. For example, multi-element antenna arrays have been used to focus energy on brain tumors, raising the local temperature to approximately 45°C in both simulations and phantom experiments [48]. Similar studies targeting breast tumors have shown that focused microwave exposure can raise tumor temperature to 42°C while maintaining surrounding healthy tissue near physiological levels (≈36°C) [49]. To enhance precision, wideband antenna designs have been proposed, providing improved field focusing compared to narrowband counterparts [50]. More recently, metasurface structures have been incorporated to further localize electromagnetic fields at depth, enabling more compact and power-efficient hyperthermia systems [51, 52]. Parallel research has also explored the use of electromagnetic fields for wireless power transfer (WPT) and communication with implantable devices, showing that conformal antennas, metasurfaces, and textile-integrated phased surfaces can improve coupling efficiency and penetration depth [53–55]. However, to the best of current knowledge,

the concept of using a passive implanted resonator to achieve localized microwave hyperthermia has not previously been proposed. This is partly because conventional superficial hyperthermia is inherently non-invasive and does not typically involve implanted structures.

Here, a passive resonator is used to concentrate EM waves at the target site, resulting in localized temperature elevation specifically at the bio-hybrid implant. Because the resonator heats more rapidly than the surrounding non-conductive medium, the temperature in adjacent tissues remains below the safety threshold of 43°C, while the bacterial colony at the implant site reaches the desired activation temperature. Simulation results indicate that this configuration can produce localized temperature increases exceeding 6°C under only 1 W of input power, which is sufficient to trigger heat-sensitive protein expression. This method thus enables precise thermal activation of genetically engineered bacteria using an external antenna.

2. WIRELESS MOLECULAR IN-BODY SENSING

2.1. Genetically Engineered Bacteria

Synthetic biology provides powerful tools for engineering bacterial cells to establish electronic communication links between living and non-living components, which can be exploited for various biosensing applications [33], [56]. Naturally, many bacterial species have evolved mechanisms to transfer electrons across their cellular membranes during anaerobic respiration, enabling them to survive by reducing metal oxides present in their environment [33], [36], [56–62]. By combining genetic circuit design approaches with protein engineering strategies, it is possible to harness these biological electron transfer pathways to develop functional bioelectronic systems [63].

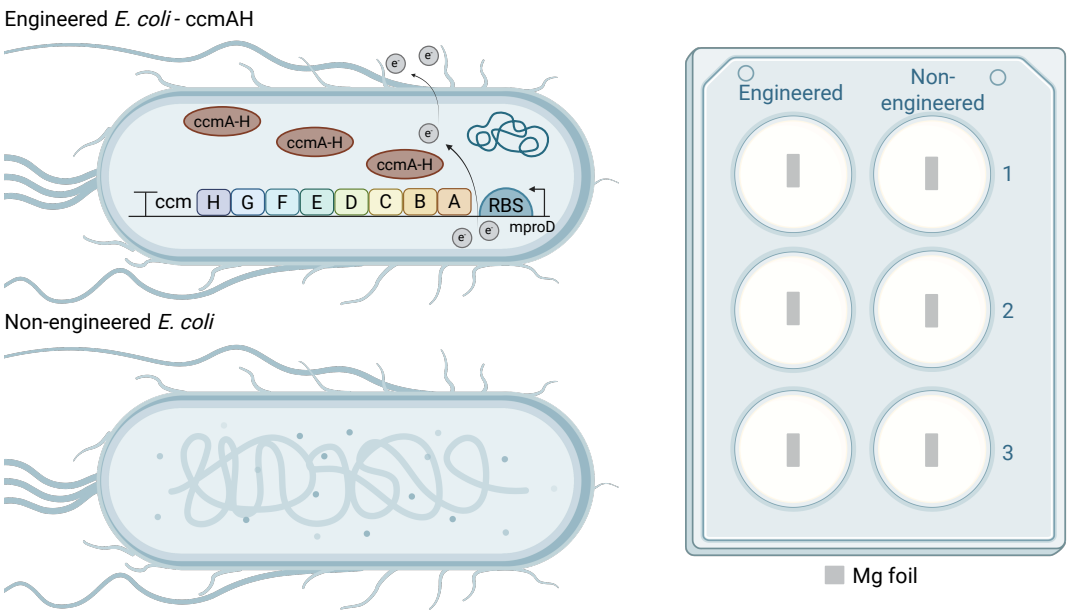

Figure 2.1. Experimental set-up comparing the activity of CcmA–H-expressing *E. coli* BL21 cells with non-engineered *E. coli* BL21. Created in BioRender.

One strategy involves constructing a synthetic electron conduit in *E. coli* by introducing and expressing a cascade of essential cytochrome proteins. This can be achieved by incorporating the genes encoding the outer-membrane cytochromes from

Shewanella oneidensis into *E.coli* and linking them to its native NapC protein (a homolog of CymA), thereby creating a continuous electron transfer pathway from the intracellular quinol pool to extracellular inorganic materials [32–34], [37], [39,40], [64,65].

In this thesis, it is envisioned that the engineered bacterial sensor will activate the expression of electron transfer proteins upon detecting a target molecule, thereby producing an electrochemical signal that can serve as a diagnostic output. To this end, *E.coli* BL21 strains were engineered to express cytochrome c maturation (CcmA–H) proteins from Shewanella oneidensis MR-1, enhancing electron flux within their electron transfer machinery [37], [64]. Genetic circuits were designed to express CcmA–H under a minimal constitutive promoter to minimize metabolic burden on the host cells. The corresponding plasmid constructs were generated using standard molecular cloning techniques, and their correctness was confirmed by sequencing. Subsequently, an experimental setup was established to compare the electrochemical activity of the CcmA–H-expressing *E. coli* BL21 strains with that of non-engineered *E. coli* BL21, as illustrated in Figure 2.1.

2.2. Degradation Speed Control

To evaluate the effectiveness of the proposed degradation speed control mechanism, an experimental setup was established as illustrated in Figure 2.2. This setup enables real-time visual monitoring of magnesium biodegradation. Rectangular magnesium foil strips (2 mm × 5 mm, 25 µm thick) were fabricated using the MITS Autolab system and placed in a six-well plate, where they were secured to the bottom of each well using biocompatible silicone. A camera positioned beneath the plate was programmed to capture images at three-minute intervals throughout the experiment. Representative images acquired at 24-hour intervals are shown in Figure 2.2.

The collected images were processed into binary format, and the remaining magnesium area was quantified by pixel counting. The results are plotted in Figure 2.3, where solid lines represent the mean pixel counts and the shaded regions indicate the

standard deviation. The data clearly show that *E. coli* BL21 CcmA–H, which constitutively expresses the introduced gene circuits, accelerates the degradation of magnesium compared to the non-engineered *E. coli* BL21 strain. This demonstrates that the expression of CcmA–H proteins enhances the biodegradation rate of magnesium foil.

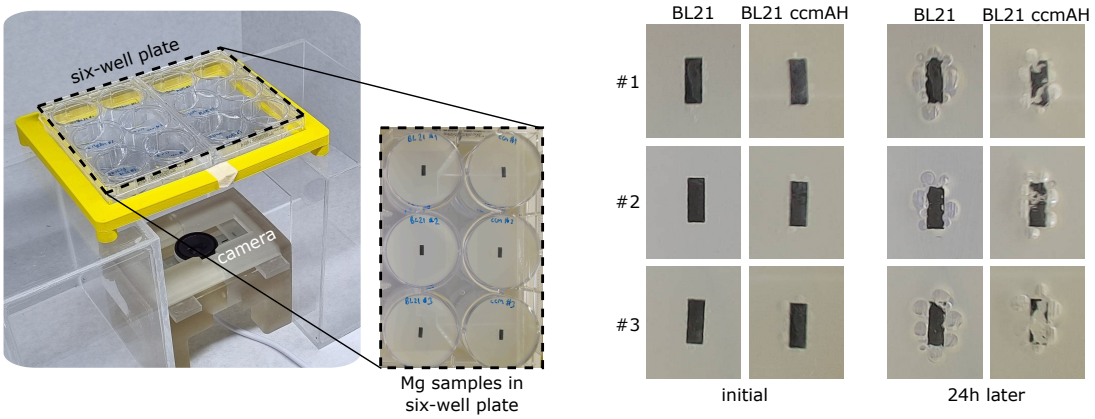

(a) (b)

Figure 2.2. (a) Experimental setup comparing the activity of engineered *E. coli* BL21 cells with non-engineered *E. coli* BL21. (b) Mg foil strips subjected to degradation experiments with *E. coli* BL21 CcmA–H, containing constitutively active gene circuits, and non-engineered *E. coli* BL21 lacking recombinant protein expression.

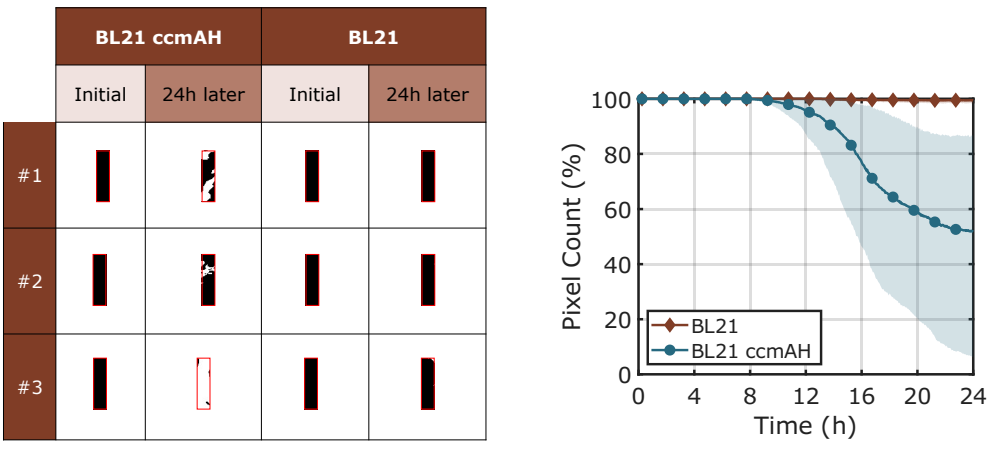

(a) (b)

Figure 2.3. (a) Binary format strip images showing the initial state and the state after 24 hours of exposure to engineered and non-engineered *E. coli* and (b) pixel counts from the binary foil images. The shaded area represents the standard deviation.

2.3. Implant Antenna Design

The passive implant antenna was designed to undergo a controlled geometrical transformation during degradation: it initially functions as a split-ring resonator and gradually transitions into a segmented-ring resonator, as illustrated in Figure 2.4. The section corresponding to the second split was designed to be 0.5 mm wide to facilitate the intended breakage point. The remaining sections were additionally covered with a protective superstrate layer to ensure that the resonant frequency evolves along a predetermined trajectory throughout the degradation process.

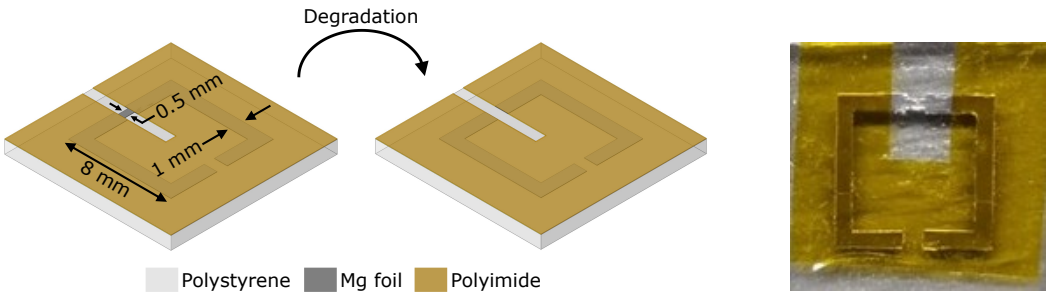

(a) (b)

Figure 2.4. (a) Design of the biodegradable passive implant antenna and its expected degradation stages, and (b) the fabricated prototype mounted on a polystyrene substrate.

To characterize its electromagnetic performance, the antenna was numerically analyzed using ANSYS HFSS in a waveguide setup, as shown in Figure 2.5. In the simulation environment, the antenna was positioned between 3-(N-morpholino)propanesulfonic acid (MOPS) and a muscle-mimicking phantom to emulate its expected configuration within the bio-hybrid implant at the system level. Frequency-dependent dielectric properties of muscle tissue were obtained from the literature [66], while the dielectric properties of MOPS were experimentally measured using a DAK SPEAG 3.5 system and incorporated into the simulation. To clearly identify the resonance behavior, the conductivity of both media was set to zero; this assumption does not influence the outcome, as the objective was to estimate the resonant frequency rather than evaluate loss characteristics. The simulated resonant frequencies of the intact and degraded

antenna structures were found to be 1.16 GHz and 1.91 GHz, respectively (Figure 2.5). The operational frequency band was selected as 1–2 GHz to balance the constraints of implantation depth and antenna size, as recommended in [67].

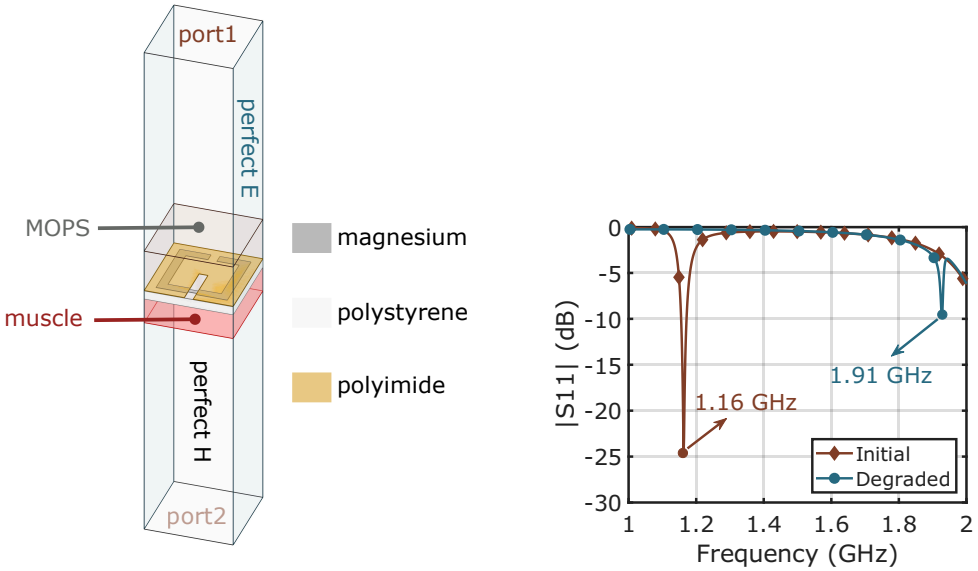

Figure 2.5. Simulation model used to determine the resonant frequency of the passive implant antenna.

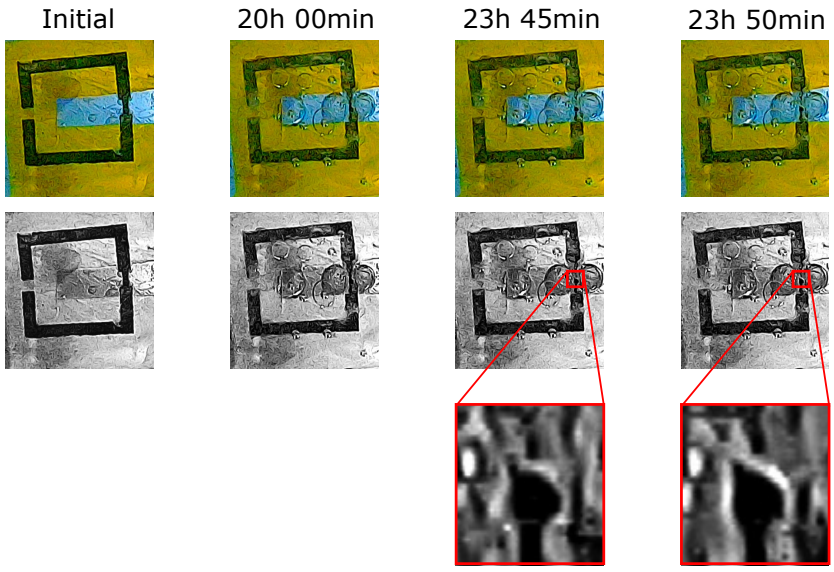

Figure 2.6. Degradation experiment of the implant antenna in MOPS medium, showing the transition from split-ring to segmented-ring geometry.

A physical prototype was fabricated using 25 µm-thick magnesium foil patterned with the MITS AutoLab. The patterned foil was mounted on an 11 mm × 11 mm, 1 mm-thick polystyrene substrate using biocompatible silicone. Polystyrene was chosen for its optical transparency, enabling visual monitoring of the degradation process to validate the wireless operation of the device.

The biodegradation behavior of the prototyped antenna in MOPS solution is presented in Figure 2.6. Time-lapse optical imaging confirmed that the structure degraded as designed. After approximately 23 hours and 50 minutes, the initial split-ring configuration transformed into a segmented ring. This transition is particularly evident in the magnified images of the 0.5 mm-wide section, verifying the controlled structural change of the antenna during degradation.

2.4. On-body Reader Antenna Design

Wearable antennas are central to a wide spectrum of biomedical applications, including off-body communication, in-body communication, wireless power transfer (WPT), and microwave imaging. Each application imposes distinct design constraints related to safety, efficiency, and usability. For off-body communication, antennas must exhibit low specific absorption rate (SAR) to ensure user safety, while maintaining flexibility and conformability for long-term wearability. In microwave imaging, in-body communication, and WPT, the primary challenge lies in achieving strong coupling between external and implanted antennas alongside sufficient electromagnetic (EM) wave penetration through biological tissues. Conformable antenna structures can improve comfort and reduce reflection losses by maintaining stable contact with the skin, but they must also preserve robust feeding performance under mechanical deformation such as bending or stretching. Furthermore, wideband operation is highly desirable, as the electrical properties of tissues vary with composition (muscle, fat, or skin), and stable performance across different body locations is critical. Dual-polarized and multi-port configurations provide additional benefits by offering polarization and spatial diversity, which reduce misalignment sensitivity and improve communication reliability.

Extensive research has focused on wearable antennas for off-body communication. Reported dual-port flexible designs include a felt-integrated antenna with orthogonal polarizations and 12 dB isolation [68], a textile-based screen-printed design providing 25 dB isolation [69], and a Taconic-substrate implementation achieving 30 dB isolation [70]. Rigid alternatives have also been explored, such as a wideband circularly polarized four-port design with 27 dB isolation [71], and a dual-port rigid antenna mounted on a flexible belt with 15 dB isolation [72]. Various single-port flexible designs have also been presented, including a wideband textile-based antenna [73], a PDMS-based circularly polarized antenna incorporating a metasurface for SAR reduction [74], and a stretchable Ecoflex-based antenna with a liquid-metal conductor and an EBG backing [75]. A strain-invariant stretchable design has also been reported [76].

Innovative materials and fabrication techniques have expanded the design space further. For example, a Kapton-based antenna using a magnetodielectric polymer for flexibility [77], and a ceramic-doped silicone substrate enabling 3D miniaturization [78] have been proposed. Additive manufacturing has also been employed, including a 3D-printed Ninjaflex/Varishore-based antenna [79] and a heterogeneous Ninjaflex–ABS structure for controlling the loss tangent [80]. Other approaches include transparent PDMS-based antennas with conductive mesh [81], and hybrid PDMS–PF4 foam substrates to reduce dielectric loss [82]. Related work has also demonstrated flexible on-body RFID tags [83, 84] and wearable sensors, such as a porous thermoplastic polyurethane-based gas sensor using carbon–nanotube–silver conductors [85].

Wearable antennas have also been widely explored for microwave imaging. Examples include textile-based wideband single-port [86], dual-port (20 dB isolation) [87], and textile-integrated [88] designs, as well as PET [89], Kapton [90], and silicone [91] substrates. Performance has been enhanced through material modifications such as iron-oxide–doped PDMS [92], alumina-doped silicone [93], and high-permittivity silicone matching layers [94]. Alongside flexible designs, several rigid microwave imaging and sensing antennas have also been reported [95–101].

For in-body communication and WPT, most reported designs are single-port and flexible. Examples include PDMS-based antennas such as a flexible phased surface for WPT [102], a flexible antenna adapted for in-body communication [103, 104], and a metamaterial-integrated wideband circularly polarized design validated on multilayer tissue [105]. Textile-based approaches include a flexible in-body communication antenna [106], a textile-integrated electronic-free phased surface for implant-to-implant communication [107], and a textile antenna to enhance coupling with deeply implanted antennas [108]. Other techniques include screen-printed textile antennas [109] and a textile-based cap antenna to power head implants [110].

Metasurface-assisted concepts have also emerged. For instance, [111] demonstrated a metasurface to enhance penetration and WPT, while [112] introduced a flexible polyimide-based metasurface, and [113] presented a wearable penetration-enhancing pad. However, these studies generally did not use direct-contact configurations. Additional works include a flexible 1×2 array on thin Rogers RT6010 (not tested across multiple tissue types) [114], a wideband flexible antenna on Rogers XT8100 characterized on multilayer tissue [115], and a flexible antenna for capsule endoscopy tracking [116].

Several rigid designs have also been investigated for WPT and in-body communication, including on-body antennas used for capsule endoscopy [117, 118], repeater antennas [119–121], pyramid-shaped ultrawideband bio-matched antennas [122–124], and a high-contrast pyramid antenna for deeper radiation [125]. Capsule endoscopy tracking antennas have been explored in [126–128], alongside pacemaker communication antennas [129], implant WPT arrays [130], and various other in-body communication designs [131–134], including a body-matched 3D-printed horn antenna [134].

Related studies have also examined the use of matching layers and metasurface structures. A dielectric matching layer to enhance penetration was introduced in [135], and a CNN-based optimization framework was proposed in [136]. A gradient refractive index metasurface was demonstrated in [137] using horn antennas, while a metasurface-integrated antenna for improved in-body links was presented in [138].

Dual-port designs for implant communication are relatively rare. A flexible polyimide-based dual-port antenna achieving 25 dB isolation was reported in [139], though only tested on homogeneous muscle tissue. A wideband dual-port rigid antenna for capsule endoscopy with 35 dB isolation was presented in [140], and a rigid dual-port pacemaker communication antenna in [141]. More recently, a wideband dual-port wearable antenna achieving 40 dB simulated isolation for in-body communication has been reported [142].

To establish the chipless RFID-based communication link between the bio-hybrid implant and the external system, a two-port on-body reader antenna was designed. On-body antennas are widely used in wearable systems and may operate in off-body, on-body, or in-body communication modes. Among these, in-body links present the greatest challenge due to strong reflections at the air–skin interface and substantial signal attenuation within tissue. Antenna performance is also highly dependent on its placement on the body, as the effective permittivity varies with local tissue composition.

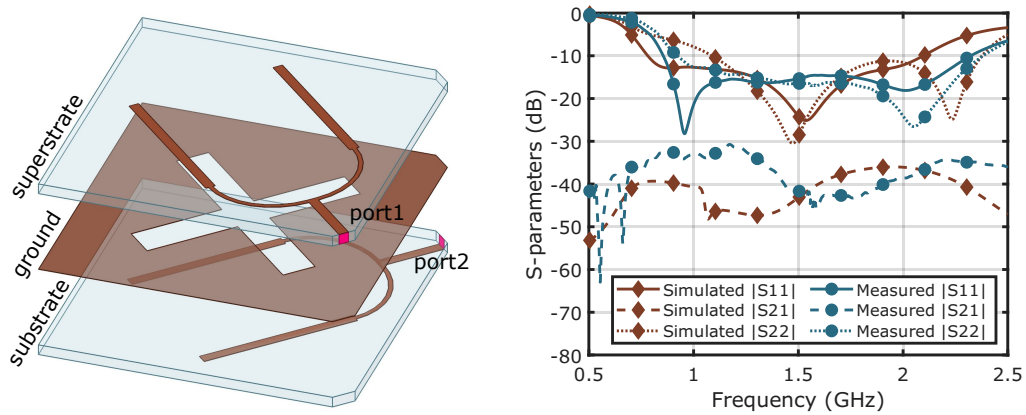

(a) (b)

Figure 2.7. (a) Geometry of the on-body reader antenna and comparison of simulated and (b) measured S-parameters when placed on muscle tissue. Solid, dashed, and dotted lines represent $|S_{11}|$, $|S_{21}|$, and $|S_{22}|$, respectively.

To maximize electromagnetic wave penetration into the body while maintaining low mutual coupling between its two ports, the reader antenna employs a cross-slot structure, as shown in Figure 2.7. The design builds upon a previously reported on-

body antenna by the authors [142]. Figure 2.7 presents both simulated and measured S-parameters when the antenna is placed on a muscle phantom. Measurements confirm that the antenna operates effectively between 0.8 GHz and 2.3 GHz, with inter-port coupling below –30 dB across this band.

2.5. Electromagnetic Simulation Results

Figure 2.8 illustrates the detailed 3D model developed for system-level simulations, along with the experimental setup and the electrical properties of both the numerical and physical phantoms. The setup consists of a plexiglass container filled with a liquid muscle-mimicking phantom. The bio-hybrid implant is placed inside a 3D-printed cup containing MOPS solution to sustain the bacterial culture, and this cup is then submerged into the muscle phantom. One side wall of the plexiglass container includes a window that serves as the interface for the on-body antenna. The on-body antenna is mounted on a 3D-printed holder, which also functions as a seal for the window. The distance between the on-body antenna and the bio-hybrid implant is fixed at 25 mm, corresponding to a representative implantation depth in the human body.

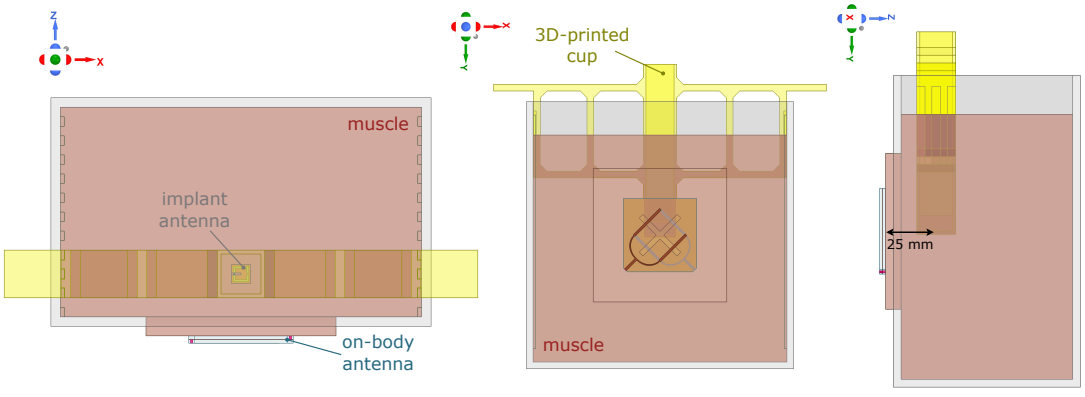

Figure 2.8. The system-level simulation model from multiple viewpoints.

System-level simulations were conducted both with and without the implant antenna present. Because muscle tissue is a highly lossy medium, the implant's response cannot be directly observed in the raw S-parameters of the on-body antenna. To isolate

the implant's response, the backscattered contribution from the surrounding environment was removed from the measured signal. This was accomplished by subtracting the transmission coefficient (S_{21}) obtained from the setup without the implant from that obtained with the implant present. This subtraction was performed in the complex domain, which is expressed as $\Delta S_{21} = S_{21,\text{with}} - S_{21,\text{without}}$. The magnitude of the calibrated transmission coefficient was then computed as $|\Delta S_{21}|(\text{dB}) = 20\log_{10}|\Delta S_{21}|$. The resulting data are shown in Figure 2.9. After calibration, a clear resonance response from the implant antenna is observed near 1.2 GHz.

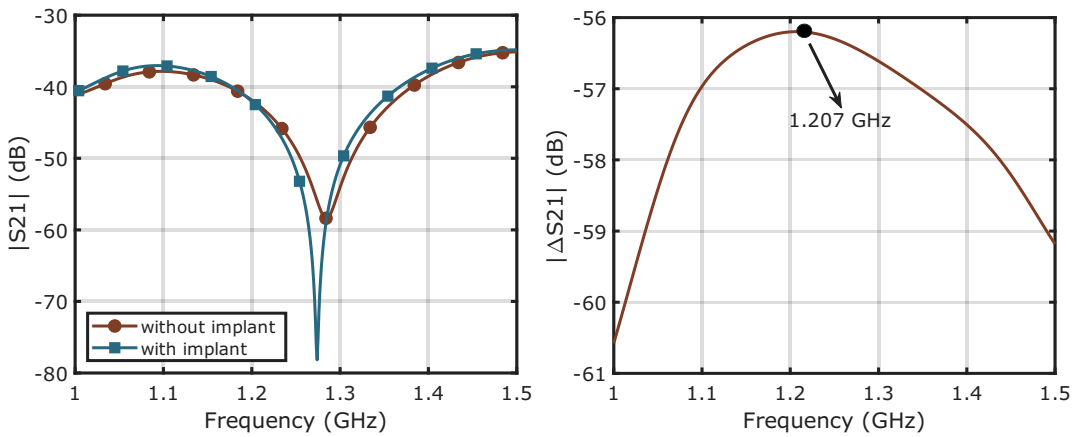

(a) (b)

Figure 2.9. Simulated transmission coefficients: (a) raw $|S_{21}|$ of the on-body antenna with and without the implant, and (b) calibrated $|S_{21}|$ after subtraction.

2.6. Phantom-Based Validation of Wireless Cell-Based Sensing

2.6.1. Measurement Setup

The measurement setup, prepared as described in Section 2.5, is shown in Figure 2.10. The on-body reader antenna was fabricated on a Rogers RO6010 substrate using an LPKF ProtoMat S103 milling machine. As the design consisted of two separate layers, three alignment holes (1 mm in diameter) were drilled into both substrates to ensure accurate registration. The two layers were then precisely aligned and bonded together using epoxy resin.

Subsequently, right-angle SMA connectors were soldered to the two antenna ports. To mount the antenna on the plexiglass container, a custom 3D-printed insert was produced using an SLA 3D printer (Anycubic Photon M3 Max) with water-washable resin. The antenna was fixed to the insert with epoxy resin, and the insert was then adhered to the plexiglass container using the same adhesive. Epoxy resin was specifically chosen to ensure a watertight seal and prevent leakage from the liquid phantom. Finally, Kapton tape was applied over the microstrip side of the antenna to prevent direct contact with the lossy liquid phantom during operation.

The implant antenna was fabricated from 99.9% pure magnesium foil with a thickness of 25 µm. The patterning process was performed using the MITS Autolab PCB prototyping machine, and the fabricated Mg structure was then mounted onto an 11 mm $\times$ 11 mm polystyrene substrate using biocompatible silicone adhesive.

Machining the Mg foil presented significant challenges due to its brittleness and extremely small thickness. The MITS Autolab operates by direct mechanical contact, which could easily fracture or tear the foil. To minimize this risk, the outline of the antenna was first lightly traced using a 60° ultramill tool without fully cutting through the foil. This approach preserved the integrity of the material during the initial shaping process and prevented unintended cracking.

After tracing, the antenna was carefully cut out along the pre-defined lines using a scalpel. It was then transferred onto a pre-shaped Kapton layer, designed to cover regions of the antenna that should remain protected from degradation. This transfer was performed with extreme care to avoid folding, tearing, or breaking the foil.

To accommodate the implant antenna and bacterial culture during experiments, a dedicated 3D-printed cup was produced using the SLA printer and water-washable resin. The cup featured side fixers that allowed it to be securely attached to the plexiglass container. Both the fixing parts and the inner surfaces of the container were equipped with interlocking male–female strips (5 mm wide) to ensure repeatable and

precise positioning of the 3D-printed cup—and therefore the implant antenna—at a consistent distance from the on-body antenna.

A camera system was also integrated into the setup to monitor the implant antenna's degradation over time. A custom 3D-printed holder was used to fix the camera in place, providing a stable and unobstructed view of the implant antenna throughout the experiment. To allow continuous optical monitoring in parallel with electromagnetic measurements, the muscle-mimicking phantom was formulated to be optically transparent, enabling simultaneous visual and RF-based observation of the implant's degradation process.

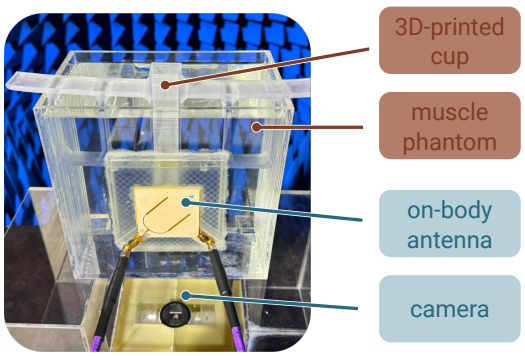

Figure 2.10. Experimental setup used for system-level measurements.

The biodegradation of the implant antenna was monitored both visually and electromagnetically. The two ports of the on-body reader antenna were connected to a vector network analyzer (VNA, Rohde & Schwarz ZNLE6). A 4K camera (Logitech MX) was positioned beneath the phantom container using a custom 3D-printed stage. Both the camera and the VNA were connected to a laptop that controlled the measurements. Complex S-parameters were recorded every five minutes over a 24-hour period, while images of the implant were captured simultaneously. The process was fully automated using a Python script. To minimize external interference, the entire setup was placed inside a 3 m $\times$ 3 m $\times$ 3 m anechoic chamber.

The muscle-mimicking phantom used in the experiments was required to be optically transparent to allow visual monitoring. It was prepared using a mixture of

deionized water, glycerol, and salt. The frequency-dependent dielectric properties of various glycerol–water mixtures are shown in Figure 2.11. The dielectric properties of the prepared phantom were compared to the reported values of human muscle tissue [66], as shown in Figure 2.12. The deviation from the target permittivity and conductivity values at 1.16 GHz were 6.6% and 15.9%, respectively.

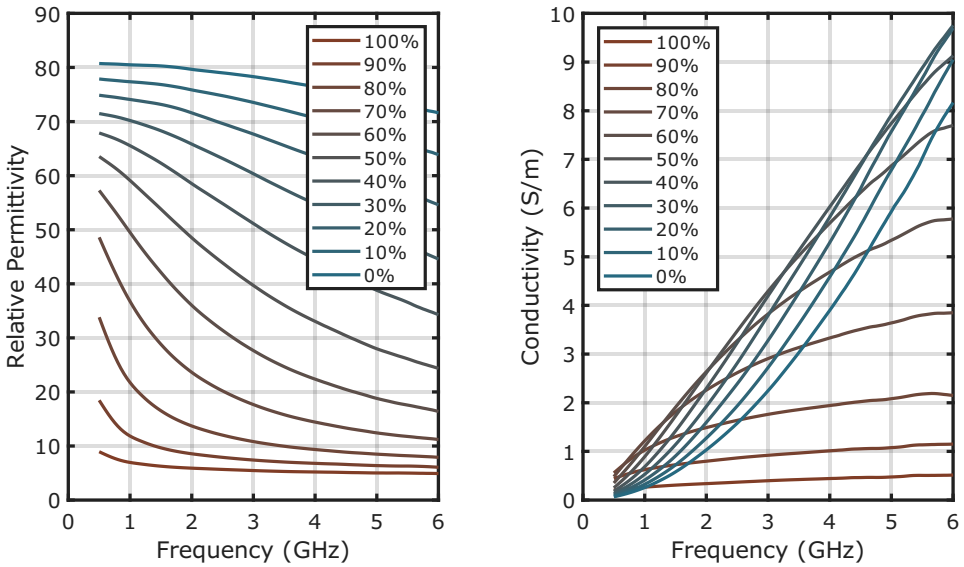

Figure 2.11. Frequency-dependent dielectric properties of glycerol–water mixtures. Percentages indicate the volume ratio of glycerol to total solution volume.

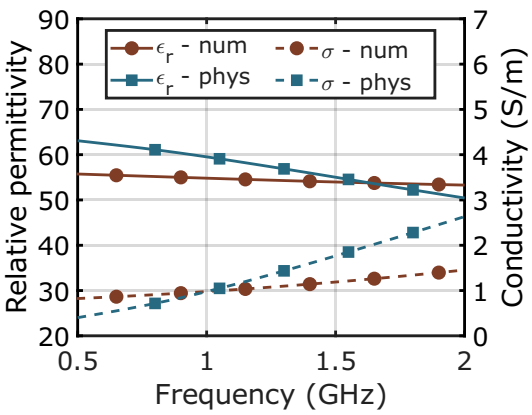

Figure 2.12. Measured dielectric properties of the numerical and physical muscle phantoms. Solid and dashed lines represent permittivity and conductivity, respectively.

2.6.2. Electromagnetic Monitoring of Biodegradation

The biodegradation process was tracked electromagnetically using the transmission coefficient between the ports of the reader antenna. The transmission coefficient measured at each time point was calibrated by subtracting the coefficient from the previous time point. It can be formulated as $\Delta S_{21}[f,n] = S_{21}[f,n] - S_{21}[f,n-1]$, which enables the detection of incremental changes. This sensing approach is based solely on detecting the presence or absence of a resonance, making it inherently immune to resonance frequency shifts caused by environmental variations around the implant.

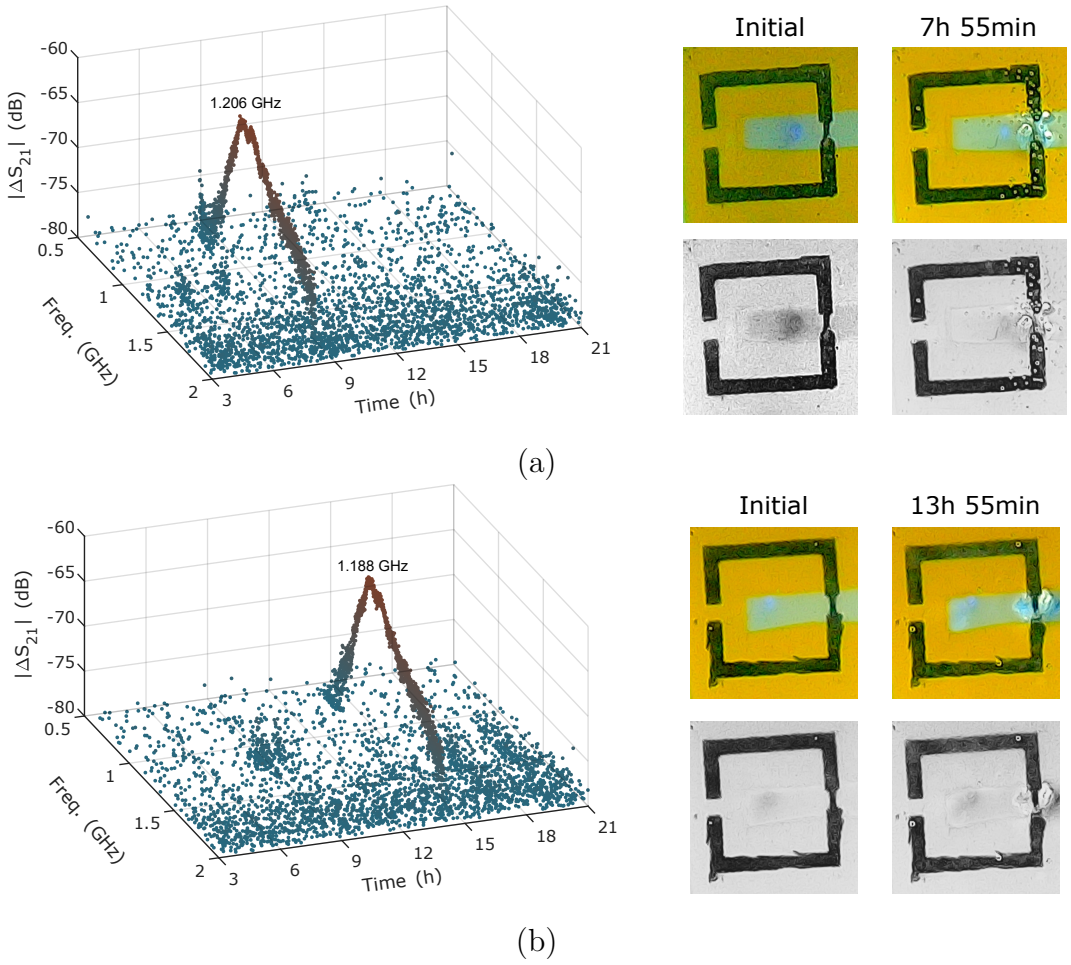

Figure 2.13. Calibrated $|S_{21}|$ values over time and visual feedback from the implant antenna during experiments with (a) engineered *E. coli* BL21 CcmA–H and (b) non-engineered *E. coli* BL21.

Figure 2.13 shows the calibrated $|S_{21}|$ values over time together with the initial and post-degradation images for both engineered *E. coli* BL21 CcmA–H and non-engineered *E. coli* BL21. The visual observations align with the electromagnetic measurements, confirming that the disconnection event seen in the images coincides with the change detected by the on-body reader antenna.

2.6.3. Measurement of Sensing Depth

To determine the maximum detectable depth of the implant antenna's resonance, additional measurements were conducted using a non-biodegradable version fabricated on an RO3003 substrate (1.57 mm thickness), shown in Figure 2.15(a). Measurements were carried out for implant depths from 25 mm to 65 mm in 10 mm increments. The same setup as in Figure 2.12 was used. To emulate the electrical properties of MOPS, a MOPS-mimicking phantom (saline solution) was used, and its dielectric properties are shown in Figure 2.14. A glycerol–water mixture was used as the muscle phantom, and its electrical properties are shown in Figure 2.11.

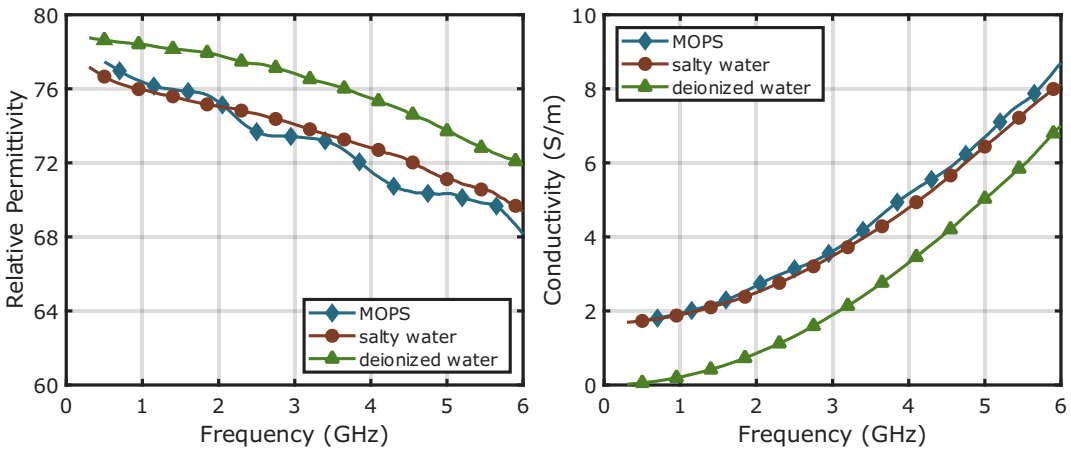

(a) (b)

Figure 2.14. Frequency-dependent (a) relative permittivity and (b) conductivity of MOPS, MOPS-mimicking phantom (salty water), and deionized water.

Each measurement consisted of three steps: (1) S-parameters were measured without the implant present, denoted as $S_{xy,1}$; (2) the implant antenna was inserted

into the 3D-printed cup and measured again, denoted as $S_{xy,2}$; (3) the implant was removed and a third measurement was taken, denoted as $S_{xy,3}$.

The first measurement ($S_{21,1}$) was used as the reference for calibration. The calibrated transmission coefficient when the implant was present was calculated as $|\Delta S_{21,2}| = |S_{21,2} - S_{21,1}|$, while the calibrated coefficient from the final measurement without the implant was computed as $|\Delta S_{21,3}| = |S_{21,3} - S_{21,1}|$, which represents the noise level.

The results are shown in Figure 2.15(b–f). As the implant depth increased, the backscattered signal from the implant weakened. The resonance remained clearly detectable up to 55 mm, while at 65 mm it was no longer visible. The slight difference in resonant frequency compared to the biodegradable version is due to the use of the non-biodegradable RO3003 substrate.

2.6.4. Effect of Medium Conductivity on Resonance Quality

To investigate the effect of the surrounding medium's conductivity on resonance quality, measurements were repeated at a fixed implant depth of 35 mm using either the MOPS-mimicking phantom or deionized water. As shown in Figure 2.14, deionized water has significantly lower conductivity. Due to the lower conductivity of the surrounding medium, the antenna exhibited a higher quality factor in deionized water, producing a sharper and more distinct resonance, as seen in Figure 2.16.

2.7. Discussion

A bio-hybrid implant composed of genetically engineered bacteria and a biodegradable antenna has been developed. The antenna was fabricated using 25 µm-thick magnesium foil, while the bacteria were engineered to modulate the biodegradation rate of the magnesium. By controlling the rate of degradation, the bacterial activity can be converted to electromagnetic signals, providing a basis for molecular-level sensing.

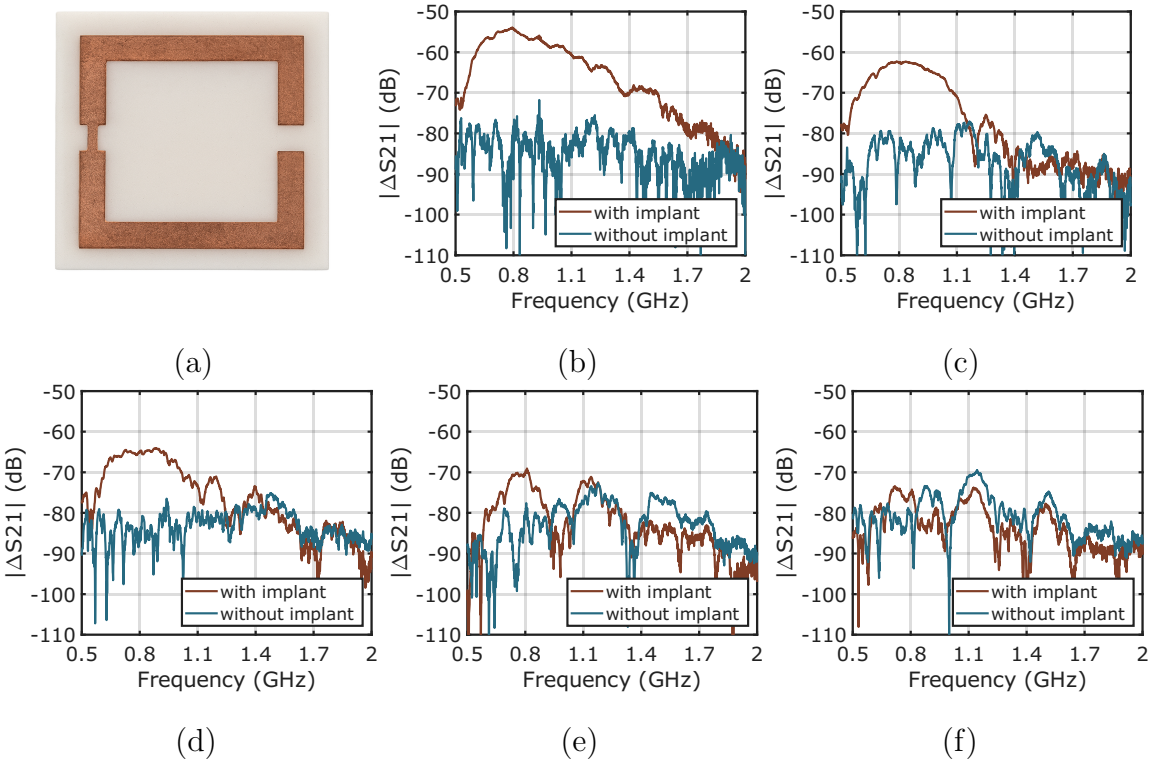

Figure 2.15. (a) Non-biodegradable implant and calibrated $|S_{21}|$ at various implant depths: (b) 25 mm, (c) 35 mm, (d) 45 mm, (e) 55 mm, and (f) 65 mm.

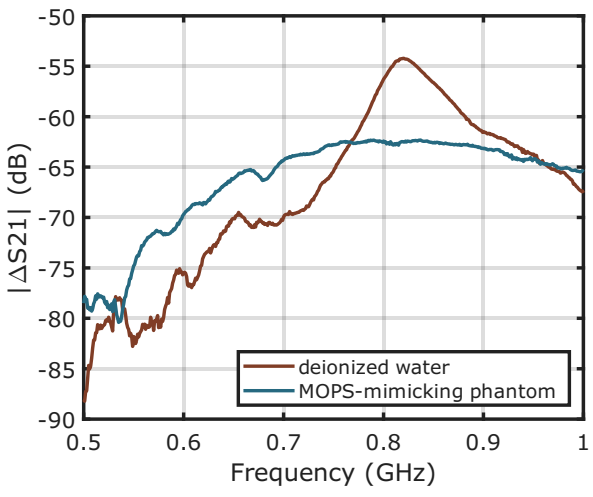

Figure 2.16. Calibrated transmission coefficients when the implant is placed in deionized water versus the MOPS-mimicking phantom (depth: 35 mm).

An on-body reader antenna, designed to operate on a muscle-mimicking phantom, covers the frequency range of the passive implant antenna throughout its degradation process. This on-body antenna enables wireless monitoring of the implant's degradation rate via backscatter communication. Using this configuration, molecular-level, cell-based sensing has been demonstrated at an implant depth of 25 mm within the muscle phantom.

In this study, *E. coli* cells were engineered to express the cytochrome c (cyt c) maturation complex (CcmA–H), enabling them to perform extracellular electron transfer (EET) and electrically interact with a metallic surface. This genetic modification creates a communication bridge between living cells and abiotic materials. Introducing EET pathways into *E.coli*—a non-native host—broadens the scope of bioelectronics by allowing the control of electron transfer rates and pathways according to application-specific needs [36], [143, 144]. Such systems hold promise as electronic "sentinel" cells for future biomedical applications.

Specifically, the *E.coli* BL21 (DE3) strain was modified to constitutively express the CcmA–H maturation pathway, thereby avoiding metabolic overload and ensuring stable performance. Experimental results showed that BL21 CcmA–H cells accelerate the degradation of magnesium compared to non-engineered BL21, reducing the degradation time from approximately 14 hours to 8 hours. The engineered bacteria were designed to enhance electron flux through expression of the cyt c protein complex, thereby facilitating controlled magnesium degradation.

Adapting a non-native host to perform EET functions presents challenges due to the complexity of native systems such as those in Geobacter and Shewanella species. To overcome this, essential components of the EET pathway were selectively introduced and optimized [36]. Prior work has shown that hybridizing the ccmH gene with the C-terminal of ccmI from S. oneidensis MR-1 can enhance EET efficiency [64]. This approach improves compatibility between the S. oneidensis cyt c system and *E.coli* [37, 64]. The hybrid CcmH protein specifically affects the inner membrane protein

CymA without altering other cyt c proteins [64]. In future implementations, this hybrid CcmH could be used in Mtr-expressing *E.coli* harboring a direct EET pathway [64]. A tunable induction system would then be required to balance the expression of the MtrCAB and Ccm pathways, ensuring proper post-translational maturation of c-type cytochromes while maintaining cell growth [39]. The resulting cyt c stoichiometry and redox activity in *E.coli* could be quantified using ferrozine assays, redox assays, or differential pulse voltammetry (DPV) [33], [145], [64].

At the system level, this work represents the first demonstration of a wireless link between a cell-based passive sensor embedded in a body-mimicking phantom and an external reader. Visual monitoring confirmed that *E.coli* BL21 CcmA–H cells degraded the magnesium implant in approximately 8 hours, whereas non-engineered BL21 cells required about 14 hours. This proof-of-concept shows that engineered cellular sensors can be integrated as electrically passive, battery-free, and circuit-free implantable devices that communicate solely through a reflector antenna.

Given the inherent capability of living cells to sense diverse biomolecules, this approach has strong potential for real-time, minimally invasive monitoring of disease progression, prognosis, and drug efficacy.

Genetically encoded cellular biosensors, especially whole-cell sensors (WCS), have emerged as powerful tools in synthetic biology due to their ability to detect and transduce environmental signals with high specificity and modularity [146, 147]. These systems rely on engineered genetic circuits composed of standardized biological parts - promoters, transcription factors, RNA-based regulators, and other elements - that can be assembled into sophisticated sensing–response modules.

Central to these circuits are genetic logic gates and state-machine architectures, which enable living cells to execute complex decision-making processes. These logic gates perform Boolean operations (AND, OR, NOT, NAND, NOR, XOR, etc.) by integrating multiple inputs (proteins, peptides, small molecules, or nucleic acids) to pro-

duce a defined output response [148,149]. Such designs typically use well-characterized genetic parts such as inducible promoters, transcriptional regulators, riboswitches, and RNA interference mechanisms to achieve predictable and tunable behavior.

One particularly promising technology is the toehold switch—a synthetic RNA-based regulatory element that provides programmable, sequence-specific translational control. Toehold switches form engineered RNA hairpins that sequester ribosome-binding sites and start codons, blocking translation until a complementary trigger RNA is present. Binding of the trigger RNA unfolds the hairpin, exposing the ribosome-binding site and initiating translation of a downstream reporter gene [150]. This mechanism allows ultra-sensitive, sequence-specific detection of nucleic acid biomarkers with minimal background noise.

Target specificity can be tailored by designing sensor components to recognize specific disease-related peptides, metabolites, or nucleic acids. Upon binding the target, the circuit can trigger a cascade of genetic events producing a measurable output signal. These outputs can be electrical—by inducing electron flow via conductive proteins such as cytochromes, metal-binding peptides, or engineered nanowires—or optical, using reporter genes encoding fluorescent proteins, luciferases, or other luminescent molecules. Electrical activity can induce localized electromagnetic changes at the cell–material interface, which could be harnessed for wireless readout. Optical signals, in contrast, offer real-time, non-invasive monitoring.

Beyond molecular recognition, biocompatibility is critical for long-term in vivo operation. To improve biocompatibility, future designs will incorporate protein-based materials and extracellular matrix (ECM)-derived biopolymers as coating layers, reducing immune responses and improving tissue integration. Signaling peptides can also be immobilized on the implant surface to promote specific cellular interactions, improve stability, and facilitate targeted signal transduction. These strategies are expected to enhance the system's long-term performance and reliability in complex biological environments.

Integrating genetic logic elements and modular sensing components within WCS provides a versatile framework for building highly specific, robust, and multifunctional biosensors. When combined with passive wireless readout, this approach can enable fully autonomous, battery-free implantable biosensing platforms. Such systems could offer real-time monitoring of physiological parameters, disease progression, and therapeutic response—all without requiring additional invasive interventions.

While the present study establishes the foundational proof-of-concept, further work is required to amplify the output signal by integrating additional molecular sensing modules and linking them to the cytochrome-based electron conduit. This will involve incorporating transcription factors and genetic regulatory systems to build more complex sensing pathways capable of generating stronger and more reliable electromagnetic responses.

3. WIRELESS ACTUATION OF GENETICALLY MODIFIED BACTERIA

3.1. Genetically Engineered Bacteria

The engineered *E. coli* strain described in [151] was used in this part of the study.

Engineered and non-engineered *E. coli* strains were cultured in 50 mL Falcon tubes containing 10 mL of LB medium. For the engineered strain, chloramphenicol (CMR) and ampicillin (AMP) were added to achieve final concentrations of 34 µg/mL and 100 µg/mL, respectively, while no antibiotics were added to the non-engineered cultures. All cultures were incubated overnight at 37°C and 200 rpm.

The following day, the overnight cultures were diluted 1:100 into fresh LB medium. For each bacterial type (engineered and non-engineered), three 10 mL cultures were prepared for the following experimental conditions:

- Incubation at 55°C for 30 minutes
- Incubation at 55°C for 60 minutes
- Continuous incubation at 37°C (control)

The diluted cultures were grown at 37°C and 200 rpm until reaching an optical density (OD_{600}) of 0.4–0.6. At this point, two engineered and two non-engineered cultures were transferred to a 55°C water bath, while the remaining one engineered and one non-engineered sample were kept at 37°C.

After 30 minutes, one engineered and one non-engineered culture were removed from the 55°C bath and returned to 37°C. The other two samples remained in the 55°C bath for an additional 30 minutes (total exposure of 60 minutes). After heat treatment, all samples were incubated at 37°C for 1 hour to allow recovery.

After the recovery period, all cultures were centrifuged at 4500 rpm for 8 minutes. The resulting pellets were resuspended in 10 mL of PBS. The Falcon tubes were sealed with parafilm and stored at +4°C overnight.

On the following day, fluorescence and absorbance measurements were performed using 3 mL cuvettes. Fluorescence was measured using an excitation wavelength of 489 nm, and emission spectra were recorded from 500 nm to 600 nm. A fluorescence peak was expected near 510 nm. For each sample, fluorescence intensity was normalized by dividing by the OD_{600} value measured in PBS.

The overall experimental workflow is illustrated in Figure 3.1.

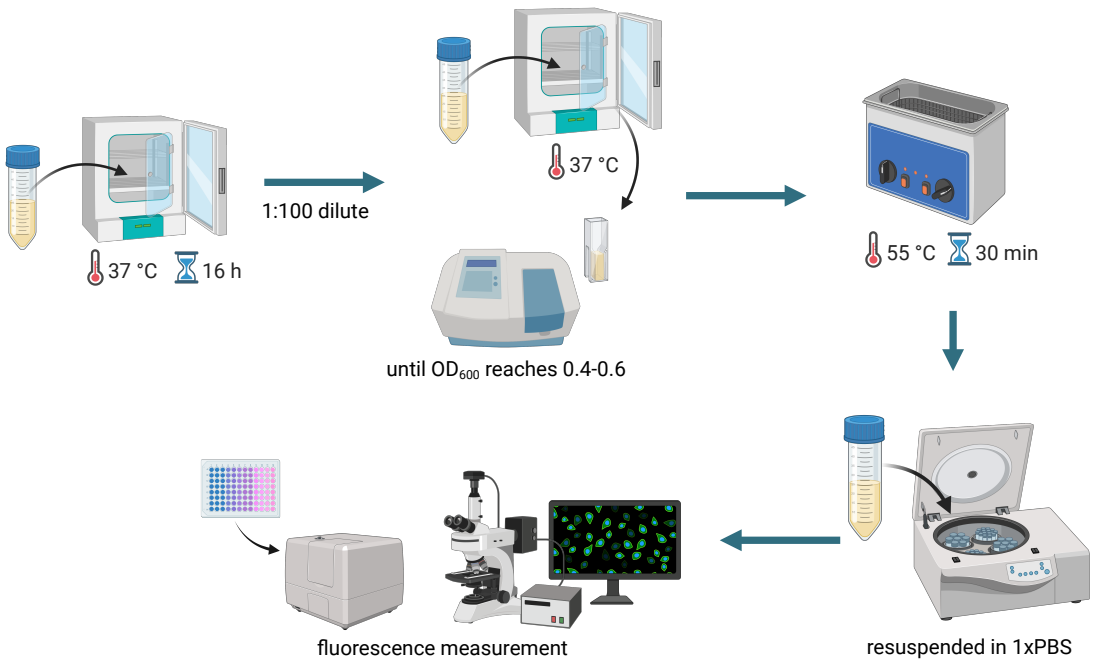

Figure 3.1. Experimental protocol for assessing the response of genetically engineered bacteria to heat exposure. Created in BioRender.

The normalized fluorescence intensities of the engineered and non-engineered bacteria incubated at 37°C are shown in Figure 3.2 (a), while the comparison of engineered bacteria subjected to different heat exposures is shown in Figure 3.2 (b).

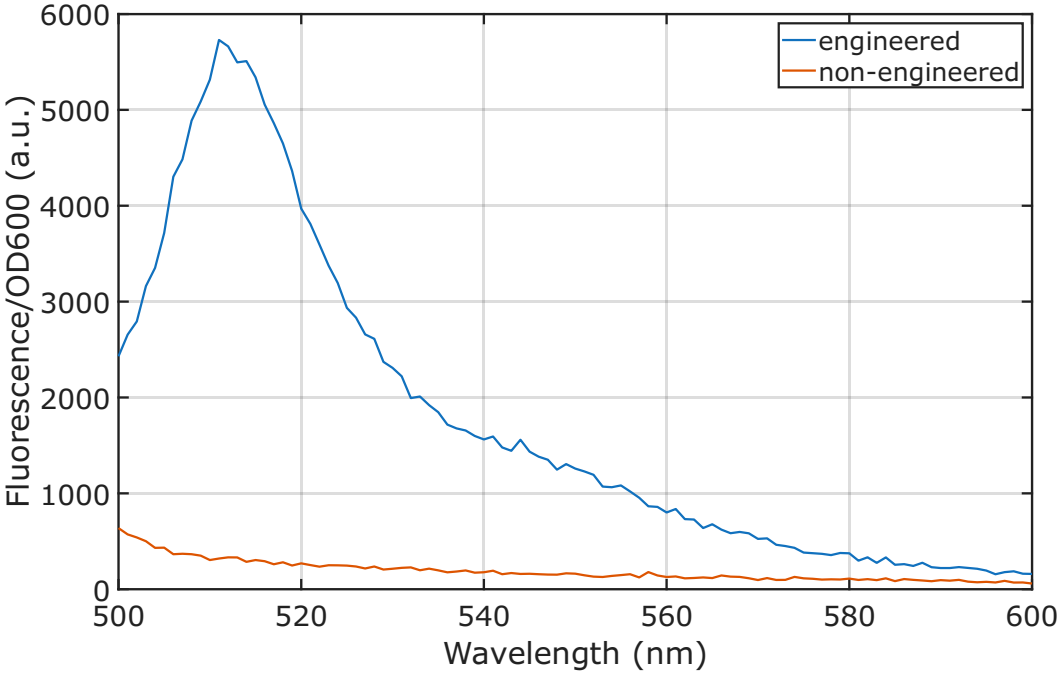

(a)

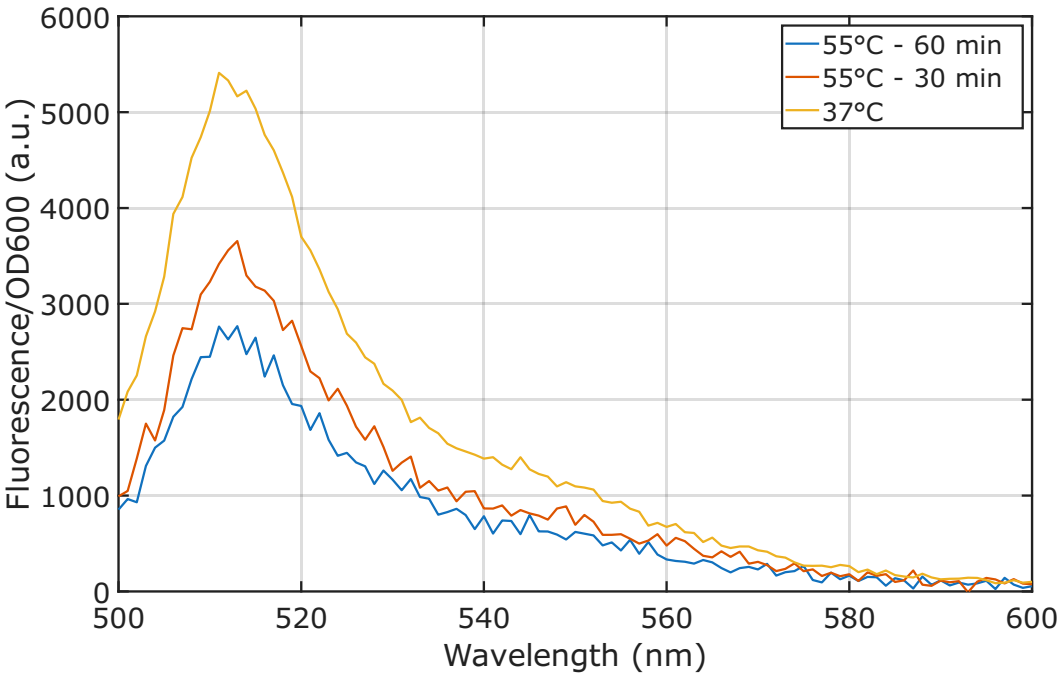

(b)

Figure 3.2. Comparison of fluorescence intensities (a) between genetically engineered and non-engineered bacteria at 37°C and (b) of the genetically engineered bacteria after different heat exposures.

Although heat exposure was expected to induce higher fluorescence in the engineered bacteria compared to non-engineered controls, this was not observed in these experiments. A likely reason is the prolonged storage of the engineered bacteria as glycerol stocks at +4°C, which may have reduced the activity of the heat-inducible genetic system. The experiment will be repeated using freshly prepared, fully functional engineered bacteria as described in [151] to validate the heat-triggered fluorescence response.

3.2. Bio-hybrid Implant

The proposed bio-hybrid implant consists of a passive implantable microwave resonator combined with a colony of genetically engineered bacteria encapsulated within a porous membrane and co-located with the resonator, as shown in Figure 3.3. The overall structure is designed as a rectangular prism with a cross section of 1 mm × 1 mm, which is suitable for minimally invasive insertion into tissue.

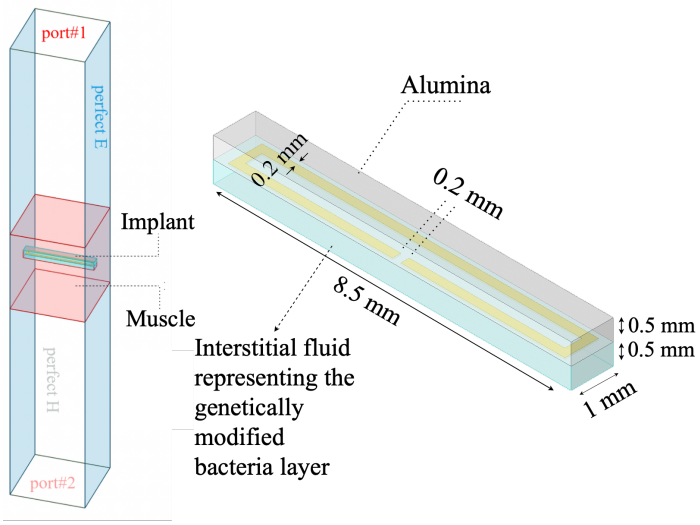

Figure 3.3. Simulation model used to determine the resonance of the implant, and schematic of the split-ring resonator integrated into the bio-hybrid implant.

The implant incorporates a split-ring resonator (SRR), which enhances local microwave absorption within the bio-hybrid construct. The resonator is patterned on

an alumina substrate and covered with a thin interstitial tissue-like layer representing the bacterial colony. This bacterial layer is modeled using the dielectric properties of extracellular fluid [152]. The complete device measures 8.5 mm × 1.0 mm × 1.0 mm, and the SRR features a 0.2 mm conductor width and 0.2 mm gap spacing.

Electromagnetic simulations were performed with the implant placed inside a waveguide (Figure 3.3). To clearly observe the resonant behavior, the conductivity values of both the surrounding muscle tissue and the interstitial fluid layer were set to zero. As shown in Figure 3.4, the resonator exhibits a distinct resonance at 1.65 GHz.

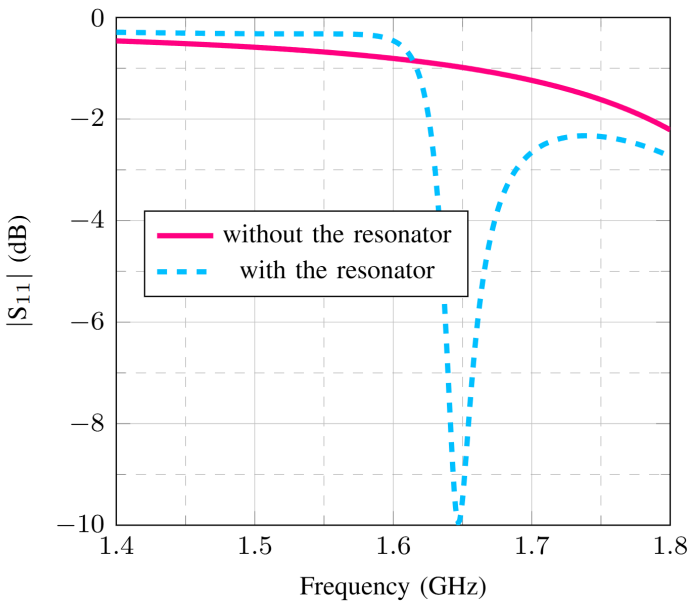

Figure 3.4. Reflection coefficient comparison of the waveguide with and without the embedded resonator present.

In this concept, genetically engineered *E. coli* are employed as the active biological component of the bio-hybrid implant. These bacteria are designed to express superfolder green fluorescent protein (sfGFP) in response to elevated temperatures. The genetic construct incorporates a heat-inducible promoter derived from bacterial heat shock response (HSR) elements [153], regulated via a transcriptional repressor system. Under normal conditions, a constitutively expressed repressor protein binds to the operator region of the promoter, blocking transcription. When the temperature

exceeds a defined threshold (typically around 42°C), the repressor dissociates, allowing RNA polymerase to initiate transcription and drive gene expression [154]. This mechanism enables the construction of sharp thermal switches that convert internal or external heat stimuli into programmable protein production [155].

This promoter–repressor logic enables precise, reversible, and highly specific control over gene expression. Similar thermal switch circuits have been widely implemented in both bacterial and phage-derived systems for spatiotemporal regulation of protein production. By tuning the dynamics of the promoter–repressor pair and adjusting the activation temperature, the system can be customized for diverse applications such as controlled therapeutic protein release or modulation of metabolic pathways.

Thermal actuation offers several advantages over conventional stimulation approaches such as chemical inducers or optogenetics. It provides a non-invasive, reversible, and spatially confined means of controlling gene expression. Moreover, thermal stimuli offer superior penetration depth in biological tissue, making them particularly suitable for in vivo biomedical applications [156].

3.3. On-body Antenna Design

A microstrip-fed wide-slot antenna was designed using ANSYS Electronics Desktop [157] to operate on muscle tissue for superficial hyperthermia applications, as shown in Figure 3.5. The antenna was optimized to maximize electromagnetic power delivery into the underlying tissue.

A magnetic-type antenna configuration was selected because of its favorable radiation characteristics near lossy biological media at sub-2 GHz frequency bands [158]. A high-permittivity substrate and superstrate were employed to minimize reflections at the air–tissue interface [159]. The high-permittivity superstrate also serves as a controlled, low-loss medium that confines the near field. This confinement reduces near-field losses within the lossy tissues, thereby improving energy transfer efficiency [142].

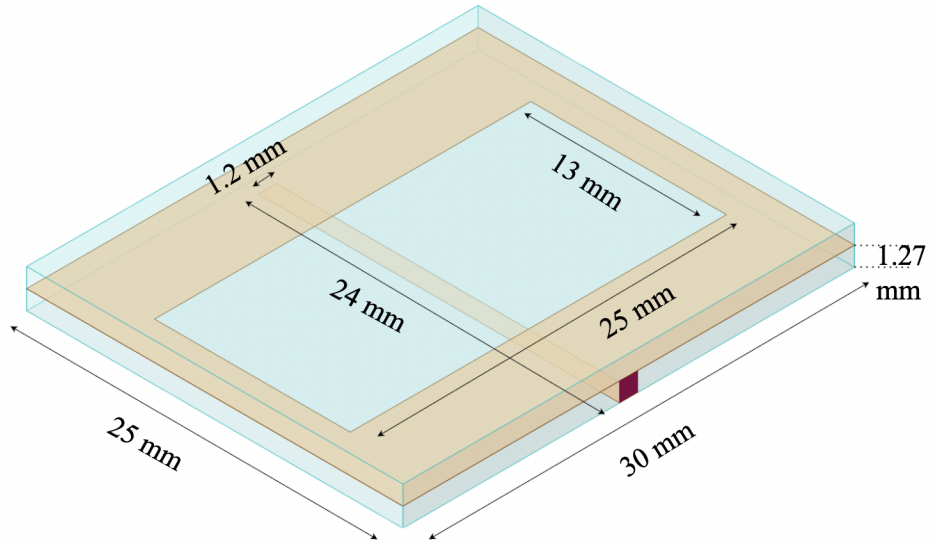

Figure 3.5. The geometry of the on-body slot antenna.

The on-body antenna was positioned on a muscle-mimicking phantom containing the bio-hybrid implant placed at a depth of 1 cm, as shown in Figure 3.6. The phantom block had dimensions of 20 cm × 20 cm × 12 cm.

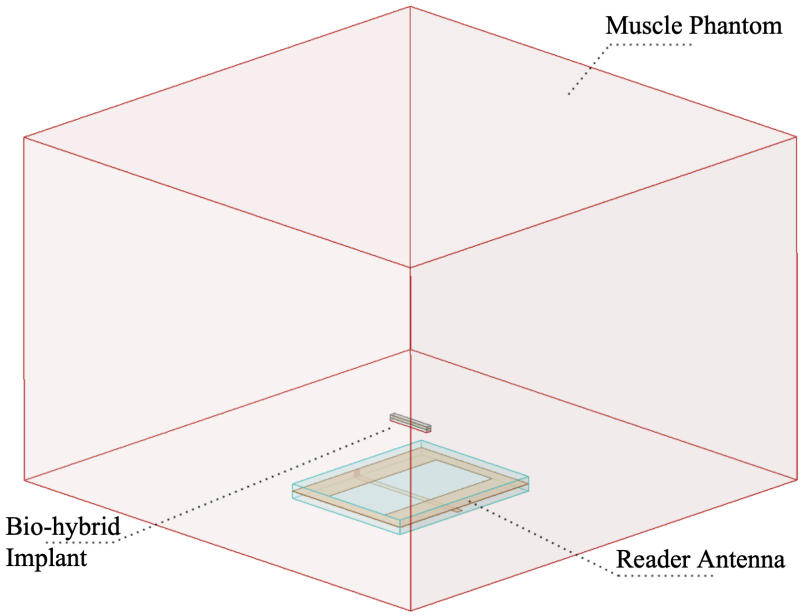

Figure 3.6. System-level simulation setup.

The return loss of the antenna was evaluated both with and without the implant present, as shown in Figure 3.7. The antenna exhibits a wide operational bandwidth from approximately 1 GHz to 2 GHz. Such wideband performance is essential, as the bio-hybrid implant may experience detuning due to tissue variability or progressive biodegradation.

The on-body antenna can efficiently transmit at the resonant frequency of the implant resonator. Notably, the resonant frequency of the implant is also visible in the return loss spectrum of the on-body antenna because the implant is located within its near field, thereby influencing the antenna's input response.

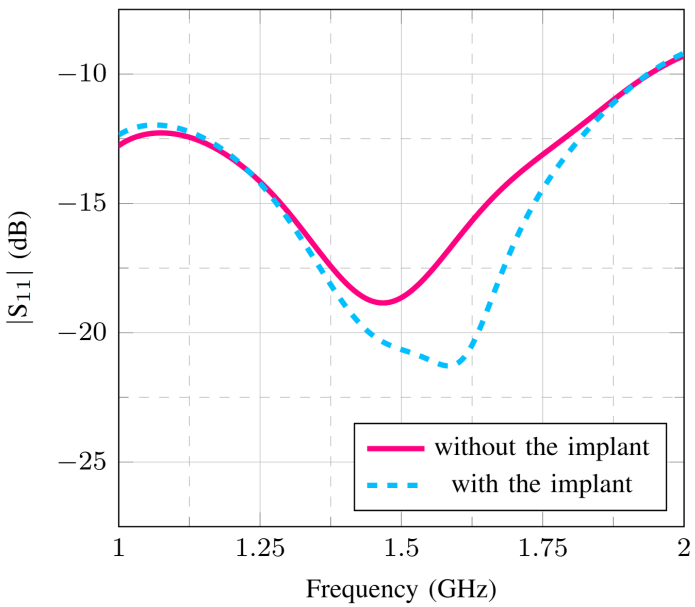

Figure 3.7. Return loss ($|S_{11}|$) of the on-body antenna measured with and without the bio-hybrid implant present.

3.4. Communication through Microwave Hyperthermia

To wirelessly control the function of the engineered bacteria, the on-body antenna must be capable of increasing the temperature of the bacterial region above the thermal activation threshold of 42°C while keeping the surrounding tissue below safe thermal limits.

Thermal simulations were performed using a multiphysics simulation tool at 1.6 GHz. The thermal properties of muscle tissue were defined as follows: density = 1047 kg/m^3, specific heat capacity = 3600 J/(kg·K), and thermal conductivity = 0.46 W/(m·K). The extracellular fluid encapsulating the bacterial colony was assumed to have the same thermal properties as muscle tissue.

The spatial distribution of the electric field is shown in Figure 3.8, comparing cases with and without the integrated resonator.

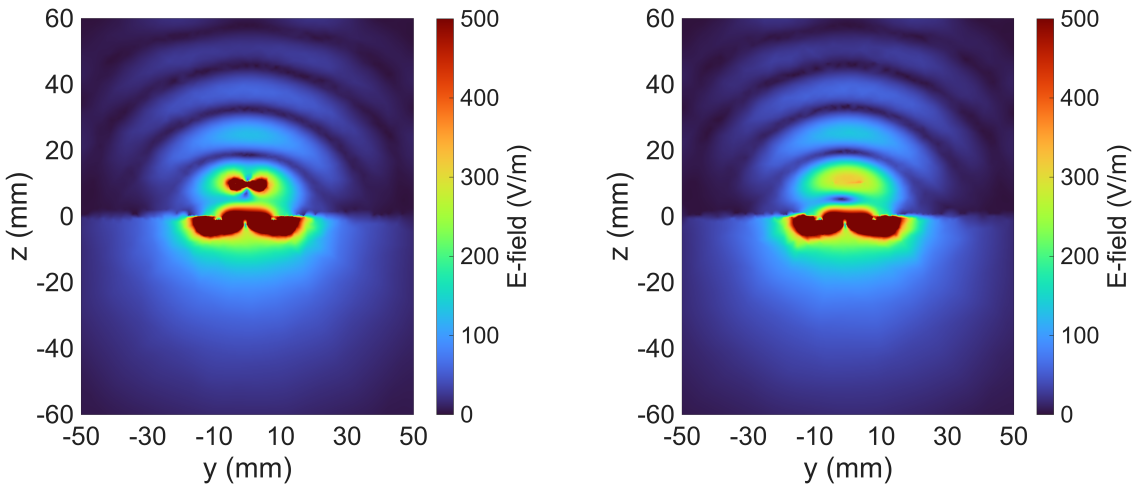

Figure 3.8. Simulated E-field distribution at 1.6 GHz: (a) with the resonator and (b) without the resonator.

Under continuous-wave excitation at 1 W input power for 5 minutes, the average temperature in the extracellular fluid volume reached 43.5°C, with a peak of 46.1°C (Figure 3.9). The maximum temperature within the surrounding muscle region remained at 42.8°C, which is below the commonly accepted safety threshold for hyperthermia.

In contrast, simulations performed without the resonator showed substantially reduced heating efficiency. The average temperature in the same extracellular fluid region reached only 40.0°C, with a maximum of 40.1°C, while the adjacent muscle

tissue warmed up to 43.3°C. This indicates more diffused and less targeted heating in the absence of the resonator.

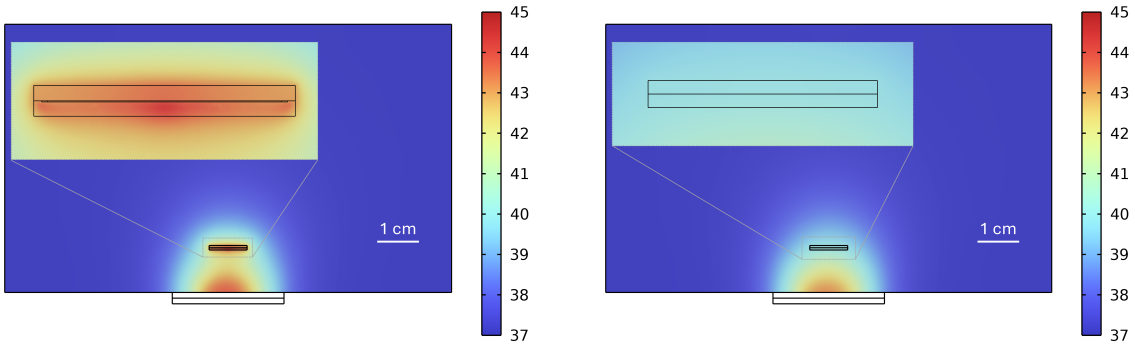

(a) (b)

Figure 3.9. Simulated temperature distribution after 5 minutes of electromagnetic heating at 1.6 GHz: (a) with and (b) without the resonator. The unit is °C.

These results confirm that the integrated resonator effectively concentrates electromagnetic energy within the implant volume, improving both heating efficiency and spatial selectivity. Once the temperature within the implant exceeds approximately 42°C, the embedded genetically engineered *E.coli* are expected to initiate the expression of target proteins. This mechanism effectively converts an external electromagnetic signal into a biological response, establishing a unidirectional communication link from the on-body antenna to the bio-hybrid implant.

Microwave hyperthermia therefore provides a wireless, non-invasive method to control synthetic cellular function without the need for any active electronics or batteries within the human body.

3.5. Future Work

The next stage of this study will focus on validating the proposed system under controlled experimental conditions. To achieve this, system-level measurements will first be conducted using a thermally sensitive phantom. This phantom will initially be optically transparent, but its opacity will increase once the temperature exceeds a de-

fined threshold, thereby providing visual feedback of local heating. This approach will allow simultaneous electromagnetic and optical monitoring, enabling direct validation of the thermal focusing capability of the system and its ability to selectively heat the implant region without significantly affecting the surrounding medium.

If the thermal phantom experiments demonstrate successful and localized heating, the same system will then be tested using the genetically engineered *E.coli*. In this phase, the bacteria will be embedded within the bio-hybrid implant, and their response to thermal stimulation will be evaluated. Fluorescence measurements will be performed to quantify the heat-induced gene expression of the engineered bacteria. This final step will confirm the complete functionality of the system, establishing a direct link between externally applied electromagnetic input, localized heating, and the resulting biological response.

4. CONCLUSION

This thesis presents the design, implementation, and validation of a bio-hybrid implant system that bridges living cells and passive antenna to achieve two complementary functionalities: wireless molecular sensing and wireless thermal actuation.

A key contribution of this work is the demonstration of a new sensing paradigm based on the integration of genetically engineered *E.coli* with a biodegradable passive implant antenna. The system translates cellular activity into electromagnetic signatures through controlled magnesium degradation, which shifts the resonant frequency of the implant. This resonance shift is wirelessly detected using an on-body dual-port antenna via backscatter communication, enabling real-time monitoring of bacterial activity without requiring any embedded electronics or batteries.

Experiments showed that engineered *E.coli* expressing cytochrome c maturation (CcmA–H) proteins accelerate magnesium corrosion compared to non-engineered controls, confirming their ability to influence the electrical behavior of the implant through extracellular electron transfer (EET). System-level measurements in muscle-mimicking phantoms further demonstrated that the implant's resonance remains detectable at depths up to 55 mm. These results validate the feasibility of using synthetic biology tools to create living, self-powered molecular sensors that can be wirelessly interrogated through external antennas.

This study also demonstrates a novel method for wirelessly controlling bacterial function using superficial microwave hyperthermia. The proposed bio-hybrid implant integrates engineered *E.coli* with a passive metallic resonator to enable localized, heat-triggered protein expression. Multiphysics simulations confirm that the system can generate a controlled temperature rise of more than 6°C at the implant site under an input power of 1 W, sufficient to activate a heat-inducible genetic circuit and initiate expression of a reporter protein. Meanwhile, the temperature in the surrounding

muscle tissue remained below the safety threshold of 43°C, confirming the spatial selectivity of the proposed approach. This establishes a unidirectional wireless link from an external antenna to the bio-hybrid implant, enabling precise control of synthetic cellular behavior without any active electronics inside the body.

Together, these findings demonstrate the feasibility of creating fully passive bioelectronic systems that combine the sensing and actuation capabilities of living cells with the wireless communication and power delivery capabilities of passive antennas. This platform eliminates the need for batteries, integrated circuits, or wired interfaces, which are major limitations of current implantable devices in terms of miniaturization, biocompatibility, and long-term stability.

Future work will focus on validating the thermal actuation concept in a thermally sensitive phantom that becomes opaque when heated, allowing real-time optical feedback. If successful, the system will then be tested with genetically engineered *E.coli* embedded within the implant, and heat-induced protein expression will be quantified through fluorescence measurements. These experiments will establish a direct link between electromagnetic input, thermal activation, and genetic response, paving the way for fully autonomous, battery-free cellular implants for real-time diagnostics and programmable therapeutics.

REFERENCES

1. Khaleghi, A., S. Dumanli and I. Balasingham., "An Overview of Medical Implant Antennas," *17th European Conference on Antennas and Propagation (EuCAP)*, Florence, Italy, pp. 1–5, 2023.

2. Koydemir, H. C. and A. Ozcan, "Wearable and Implantable Sensors for Biomedical Applications," *Annual Review of Analytical Chemistry*, vol. 11, no. 1, pp. 127–146, 2018.

3. Gray, M., J. Meehan, C. Ward, S. P. Langdon, I. H. Kunkler, A. Murray and D. Argyle, "Implantable Biosensors and Their Contribution to the Future of Precision Medicine," *Veterinary Journal*, vol. 239, pp. 21–29, 2018.

4. Veletić, M., E. H. Apu, M. Simić, J. Bergsland, I. Balasingham, C. H. Contag and N. Ashammakhi, "Implants with Sensing Capabilities," *Chemical Reviews*, vol. 122, no. 21, pp. 16329–16363, 2022.

5. Goncalves, A. D., W. Balestri and Y. Reinwald, "Biomedical Implants for Regenerative Therapies," in *Biomaterials*, IntechOpen, London, pp. 1-36, 2020.

6. Cil, E., I. V. Soares, D. Renaudeau, R. Lucas, S. Dumanli, R. Sauleau and D. Nikolayev, "On the Use of Impedance Detuning for Gastrointestinal Segment Tracking of Ingestible Capsules," *IEEE Transactions on Antennas and Propagation*, vol. 71, no. 2, pp. 1977–1981, 2023.

7. Lozano, A. M., N. Lipsman, H. Bergman, P. Brown, S. Chabardes, J. W. Chang, K. Matthews, C. C. McIntyre, T. E. Schlaepfer, M. Schulder, Y. Temel, J. Volkmann and J. K. Krauss, "Deep Brain Stimulation: Current Challenges and Future Directions," *Nature Reviews Neurology*, vol. 15, no. 3, pp. 148–160, 2019.

8. Villena Gonzales, W., A. Mobashsher and A. Abbosh, "The Progress of Glucose

Monitoring—A Review of Invasive to Minimally and Non-Invasive Techniques, Devices and Sensors," *Sensors*, vol. 19, no. 4, p. 800, 2019.

9. Lucisano, J. Y., T. L. Routh, J. T. Lin and D. A. Gough, "Glucose Monitoring in Individuals With Diabetes Using a Long-Term Implanted Sensor/Telemetry System and Model," *IEEE Transactions on Biomedical Engineering*, vol. 64, no. 9, pp. 1982–1993, 2017.

10. Gonzalez-Guillaumin, L., D. C. Sadowski, K. V. I. S. Kaler and M. P. Mintchev, "Ingestible Capsule for Impedance and pH Monitoring in the Esophagus," *IEEE Transactions on Biomedical Engineering*, vol. 54, no. 12, pp. 2231–2236, 2007.

11. Chen, X., D. Brox, B. Assadsangabi, Y. Hsiang and K. Takahata, "Intelligent Telemetric Stent for Wireless Monitoring of Intravascular Pressure and Its In Vivo Testing," *Biomedical Microdevices*, vol. 16, no. 5, pp. 745–759, 2014.

12. Malik, J., S. Kim, J. M. Seo, Y. M. Cho and F. Bien, "Minimally Invasive Implant Type Electromagnetic Biosensor for Continuous Glucose Monitoring System: In Vivo Evaluation," *IEEE Transactions on Biomedical Engineering*, vol. 70, no. 3, pp. 1000–1011, 2023.

13. Erden, O. K., A. Bilir, C. Karabulut, U. O. Safak Seker and S. Dumanli, "Antennas Reconfigured by Living Cells: AntennAlive," *IEEE International Symposium on Antennas and Propagation and USNC-URSI Radio Science Meeting (AP-S/URSI)*, Denver, CO, USA, pp. 882–883, 2022.

14. Koksaldi, I. C. *et al.*, "Genetically engineered bacterial biofilm materials enhances portable whole cell sensing," *Biosensors and Bioelectronics*, vol. 264, p. 116644, 2024.

15. Kose, S. *et al.*, "Multiplexed cell-based diagnostic devices for detection of renal biomarkers," *Biosensors and Bioelectronics*, vol. 223, p. 115035, 2023.

16. Karabulut, C., A. Bilir, M. E. Lacin and S. Dumanli, "3D-Engineered Muscle Tissue as a Wireless Sensor: AntennAlive [Bioelectromagnetics]," *IEEE Antennas and Propagation Magazine*, vol. 65, no. 6, pp. 28–36, 2023.

17. Thévenot, D. R., K. Toth, R. A. Durst and G. S. Wilson, "Electrochemical Biosensors: Recommended Definitions and Classification," *Biosensors and Bioelectronics*, vol. 16, no. 1–2, pp. 121–131, 2001.

18. Maccaferri, N., K. E. Gregorczyk, T. V. A. G. de Oliveira, M. Kataja, S. van Dijken, Z. Pirzadeh, A. Dmitriev, J. Åkerman, M. Knez and P. Vavassori, "Ultrasensitive and Label-free Molecular-level Detection Enabled by Light Phase Control in Magnetoplasmonic Nanoantennas," *Nature Communications*, vol. 6, no. 1, Art. no. 6150, 2015.

19. Cash, K. J., F. Ricci and K. W. Plaxco, "An Electrochemical Sensor for the Detection of Protein–Small Molecule Interactions Directly in Serum and Other Complex Matrices," *Journal of the American Chemical Society*, vol. 131, no. 20, pp. 6955–6957, 2009.

20. Saunders, J., I. A. Thompson and H. T. Soh, "Generalizable Molecular Switch Designs for In Vivo Continuous Biosensing," *Accounts of Chemical Research*, vol. 58, no. 5, pp. 703–713, 2025.

21. Chen, Y. *et al.*, "A Biochemical Sensor with Continuous Extended Stability In Vivo," *Nature Biomedical Engineering*, vol. 9, no. 9, pp. 1517–1530, 2025.

22. Moutsiopoulou, A., D. Broyles, E. Dikici, S. Daunert and S. K. Deo, "Molecular Aptamer Beacons and Their Applications in Sensing, Imaging, and Diagnostics," *Small*, vol. 15, no. 35, Art. no. e1902248, 2019.

23. Chien, J.-C., S. W. Baker, K. Gates, J.-W. Seo, A. Arbabian and H. T. Soh, "Wireless Monitoring of Small Molecules on a Freely-Moving Animal Using Electro-

chemical Aptamer Biosensors," *IEEE Biomedical Circuits and Systems Conference (BioCAS)*, Taipei, Taiwan, pp. 36–39, 2022.

24. Chen, S., T.-L. Liu, Y. Dong and J. Li, "A Wireless, Regeneratable Cocaine Sensing Scheme Enabled by Allosteric Regulation of pH Sensitive Aptamers," *ACS Nano*, vol. 16, no. 12, pp. 20922–20936, 2022.

25. Benner, S. A. and A. M. Sismour, "Synthetic Biology," *Nature Reviews Genetics*, vol. 6, no. 7, pp. 533–543, 2005.

26. Balci, B. and P. Dincer, "Efficient Transfection of Mouse-Derived C2C12 Myoblasts Using a Matrigel Basement Membrane Matrix," *Biotechnology Journal*, vol. 4, no. 7, pp. 1042–1045, 2009.

27. Sezgen, O. F., O. Altan, A. Bilir, M. G. Durmaz, N. Haciosmanoglu, B. Camli, Z. C. C. Ozdil, A. E. Pusane, A. D. Yalcinkaya, U. O. Safak Seker, T. Tugcu and S. Dumanli, "A Multiscale Communications System Based on Engineered Bacteria," *IEEE Communications Magazine*, vol. 59, no. 5, pp. 62–67, 2021.

28. Gupta, N., V. Renugopalakrishnan, D. Liepmann, R. Paulmurugan and B. D. Malhotra, "Cell-based Biosensors: Recent Trends, Challenges and Future Perspectives," *Biosensors and Bioelectronics*, vol. 141, p. 111435, 2019.

29. Saltepe, B., E. S. Kehribar, S. S. Su Yirmibesoglu and U. O. Safak Seker, "Cellular Biosensors with Engineered Genetic Circuits," *ACS Sensors*, vol. 3, no. 1, pp. 13–26, 2018.

30. Koirala, G. R. *et al.*, "Fully Wireless, In Vivo Assessment of Superimposed Physiological Vital Signs Using a Biodegradable Passive Tag Interrogated with a Wearable Reader Patch," *Advanced Functional Materials*, vol. 35, no. 3, Art. no. 2413363, 2024.

31. Mariello, M. *et al.*, "Wireless, Battery-Free, and Real-Time Monitoring of Water

Permeation Across Thin-Film Encapsulation," *Nature Communications*, vol. 15, no. 1, Art. no. 7443, 2024.

32. Bird, L. J. *et al.*, "Engineering Wired Life: Synthetic Biology for Electroactive Bacteria," *ACS Synthetic Biology*, vol. 10, no. 11, pp. 2808–2823, 2021.

33. Jensen, H. M. *et al.*, "Engineering of a Synthetic Electron Conduit in Living Cells," *Proceedings of the National Academy of Sciences*, vol. 107, no. 45, pp. 19213–19218, 2010.

34. Baruch, M., S. Tejedor-Sanz, L. Su and C. M. Ajo-Franklin, "Electronic Control of Redox Reactions Inside *E. coli* Using a Genetic Module," *PLoS One*, vol. 16, no. 11, p. e0258380, 2021.

35. Oktar, S. D., "A System and Method Which Provides Wireless Communication Between Bio-nano Elements and Macro/micro Devices," U.S. Patent WO2021126135A1, 2021. Available: https://patents.google.com/patent/WO2021126135A1, Accessed on September 15, 2025.

36. Jensen, H. M., M. A. TerAvest, M. G. Kokish and C. M. Ajo-Franklin, "CymA and Exogenous Flavins Improve Extracellular Electron Transfer and Couple It to Cell Growth in Mtr-expressing *E. coli*," *ACS Synthetic Biology*, vol. 5, no. 7, pp. 679–688, 2016.

37. Su, L., T. Fukushima, A. Prior, M. Baruch, T. J. Zajdel and C. M. Ajo-Franklin, "Modifying Cytochrome c Maturation Can Increase the Bioelectronic Performance of Engineered *E. coli*," *ACS Synthetic Biology*, vol. 9, no. 1, pp. 115–124, 2020.

38. Ikeda, S. *et al.*, "*Shewanella oneidensis* MR-1 as a Bacterial Platform for Electro-Biotechnology," *Essays in Biochemistry*, vol. 65, no. 2, pp. 355–364, 2021.

39. Goldbeck, C. P. *et al.*, "Tuning Promoter Strengths for Improved Synthesis and

Function of Electron Conduits in *E. coli*," *ACS Synthetic Biology*, vol. 2, no. 3, pp. 150–159, 2013.

40. TerAvest, M. A., T. J. Zajdel and C. M. Ajo-Franklin, "The Mtr Pathway of *Shewanella oneidensis* MR-1 Couples Substrate Utilization to Current Production in *E. coli*," *ChemElectroChem*, vol. 1, no. 11, pp. 1874–1879, 2014.

41. Schuergers, N., C. Werlang, C. M. Ajo-Franklin and A. A. Boghossian, "A Synthetic Biology Approach to Engineering Living Photovoltaics," *Energy and Environmental Science*, vol. 10, no. 5, pp. 1102–1115, 2017.

42. Zhang, D., Q. Chen, C. Shi, M. Chen and K. Ma, "Dealing with the Foreign-body Response to Implanted Biomaterials: Strategies and Applications of New Materials," *Advanced Functional Materials*, vol. 31, no. 4, p. 2007226, 2021.

43. Bilir, A. and S. Dumanli, "Biodegradable Implant Antenna Utilized for Real-Time Sensing Through Genetically Modified Bacteria," *18th European Conference on Antennas and Propagation (EuCAP)*, Glasgow, United Kingdom, pp. 1–4, 2024.

44. Jornet, J. M. and I. F. Akyildiz, "Channel Modeling and Capacity Analysis for Electromagnetic Wireless Nanonetworks in the Terahertz Band," *IEEE Transactions on Wireless Communications*, vol. 10, no. 10, pp. 3211–3221, 2011.

45. Gabriel, S., R. W. Lau and C. Gabriel, "The Dielectric Properties of Biological Tissues: II. Measurements in the Frequency Range 10 Hz to 20 GHz," *Physics in Medicine and Biology*, vol. 41, no. 11, pp. 2251–2269, 1996.

46. Chatterjee, D. K., P. Diagaradjane and S. Krishnan, "Nanoparticle-mediated Hyperthermia in Cancer Therapy," *Therapeutic Delivery*, vol. 2, no. 8, pp. 1001–1014, 2011.

47. Wu, J. *et al.*, "Non-invasive Differential Temperature Monitoring Using Sensor Array for Microwave Hyperthermia Applications: A Subspace-based Approach,"

Journal of Sensor and Actuator Networks, vol. 14, no. 1, p. 19, 2025.

48. Xi, Z. *et al.*, "A Preclinical System Prototype and Experimental Validation of Focused Microwave Brain Hyperthermia," *IEEE Transactions on Microwave Theory and Techniques*, vol. 73, no. 2, pp. 1147–1157, 2025.

49. Nguyen, P. T., A. M. Abbosh and S. Crozier, "3-D Focused Microwave Hyperthermia for Breast Cancer Treatment with Experimental Validation," *IEEE Transactions on Antennas and Propagation*, vol. 65, no. 7, pp. 3489–3500, 2017.

50. Converse, M. *et al.*, "A Computational Study of Ultra-wideband Versus Narrowband Microwave Hyperthermia for Breast Cancer Treatment," *IEEE Transactions on Microwave Theory and Techniques*, vol. 54, no. 5, pp. 2169–2180, 2006.

51. Hajiahmadi, M. J., R. Faraji-Dana and C. Caloz, "Metasurface-based Time-reversal Focusing for Brain Tumor Microwave Hyperthermia," *IEEE Transactions on Antennas and Propagation*, vol. 70, no. 12, pp. 12237–12246, 2022.

52. Xiong, H. *et al.*, "Microwave Hyperthermia Technology Based on Near-field Focused Metasurfaces: Design and Implementation," *Advanced Functional Materials*, vol. 35, no. 1, Art. no. 2411842, 2024.

53. Soares, I. V. *et al.*, "Wireless Powering Efficiency of Deep-body Implantable Devices," *IEEE Transactions on Microwave Theory and Techniques*, vol. 71, no. 6, pp. 2680–2692, 2023.

54. Shah, I. A. *et al.*, "Flexible Metasurface-coupled Efficient Wireless Power Transfer System for Implantable Devices," *IEEE Transactions on Microwave Theory and Techniques*, vol. 72, no. 4, pp. 2534–2547, 2024.

55. Tian, X. *et al.*, "Textile-integrated Phased Surfaces for Wireless Networking of Bioelectronic Devices," *IEEE Transactions on Antennas and Propagation*, vol. 72, no. 1, pp. 267–276, 2024.

56. Ueki, T., L. N. DiDonato and D. R. Lovley, "Toward Establishing Minimum Requirements for Extracellular Electron Transfer in *Geobacter sulfurreducens*," *FEMS Microbiology Letters*, vol. 364, no. 9, 2017.

57. West, E. A., A. Jain and J. A. Gralnick, "Engineering a Native Inducible Expression System in *Shewanella oneidensis* to Control Extracellular Electron Transfer," *ACS Synthetic Biology*, vol. 6, no. 9, pp. 1627–1634, 2017.

58. Shi, L. *et al.*, "Extracellular Electron Transfer Mechanisms Between Microorganisms and Minerals," *Nature Reviews Microbiology*, vol. 14, no. 10, pp. 651–662, 2016.

59. Shi, L. *et al.*, "The Roles of Outer Membrane Cytochromes of *Shewanella* and *Geobacter* in Extracellular Electron Transfer," *Environmental Microbiology Reports*, vol. 1, no. 4, pp. 220–227, 2009.

60. Marritt, S. J. *et al.*, "A Functional Description of CymA, an Electron-Transfer Hub Supporting Anaerobic Respiratory Flexibility in *Shewanella*," *Biochemical Journal*, vol. 444, no. 3, pp. 465–474, 2012.

61. Sturm, G. *et al.*, "A Dynamic Periplasmic Electron Transfer Network Enables Respiratory Flexibility Beyond a Thermodynamic Regulatory Regime," *The ISME Journal*, vol. 9, no. 8, pp. 1802–1811, 2015.

62. Hartshorne, R. S. *et al.*, "Characterization of an Electron Conduit Between Bacteria and the Extracellular Environment," *Proceedings of the National Academy of Sciences*, vol. 106, no. 52, pp. 22169–22174, 2009.

63. Kalyoncu, E., R. E. Ahan, T. T. Olmez and U. O. Safak Seker, "Genetically Encoded Conductive Protein Nanofibers Secreted by Engineered Cells," *RSC Advances*, vol. 7, no. 52, pp. 32543–32551, 2017.

64. Su, L., T. Fukushima and C. M. Ajo-Franklin, "A Hybrid Cyt c Maturation System

Enhances the Bioelectrical Performance of Engineered *E. coli* by Improving the Rate-Limiting Step," *Biosensors and Bioelectronics*, vol. 165, p. 112312, 2020.

65. Lienemann, M. *et al.*, "Towards Patterned Bioelectronics: Facilitated Immobilization of Exoelectrogenic *E. coli* with Heterologous Pili," *Microbial Biotechnology*, vol. 11, no. 6, pp. 1184–1194, 2018.

66. Gabriel, C., "Compilation of the Dielectric Properties of Body Tissues at RF and Microwave Frequencies," Occupational and Environmental Health Directorate, Radiofrequency Radiation Division, Brooks Air Force Base, TX, USA, Report N. AL/OE-TR-1996-0037, 1996.

67. Skrivervik, A. K., M. Bosiljevac and Z. Sipus, "Antennas for Implants: Design and Limitations," in *Bioelectromagnetics in Healthcare: Advanced Sensing and Communication Applications*, W. Whittow, Ed., Stevenage, U.K.: IET, pp. 81–90, 2022.

68. Li, H., S. Sun, B. Wang and F. Wu, "Design of Compact Single-Layer Textile MIMO Antenna for Wearable Applications," *IEEE Transactions on Antennas and Propagation*, vol. 66, no. 6, pp. 3136–3141, 2018.

69. Mao, C. X., Y. Zhou, Y. Wu, H. Soewardiman, D. H. Werner and J. S. Jur, "Low-profile Strip-loaded Textile Antenna with Enhanced Bandwidth and Isolation for Full-duplex Wearable Applications," *IEEE Transactions on Antennas and Propagation*, vol. 68, no. 9, pp. 6527–6537, 2020.

70. Wu, Y., G. Mackertich-Sengerdy, S. Soltani, S. D. Campbell, D. Yang and D. H. Werner, "Low Profile Orthomode Full-duplex Antenna for Wearable Biomedical Communication," *IEEE Access*, vol. 12, pp. 40092–40104, 2024.

71. Iqbal, A., A. Smida, A. J. Alazemi, M. I. Waly, N. Khaddaj Mallat and S. Kim, "Wideband Circularly Polarized MIMO Antenna for High Data Wearable Biotelemetric Devices," *IEEE Access*, vol. 8, pp. 17935–17944, 2020.

72. Yang, S., L. Zhang, W. Wang and Y. Zheng, "Flexible Tri-band Dual-polarized MIMO Belt Strap Antenna Toward Wearable Applications in Intelligent Internet of Medical Things," *IEEE Transactions on Antennas and Propagation*, vol. 70, no. 1, pp. 197–208, 2022.

73. Samal, P. B., S. J. Chen and C. Fumeaux, "Wearable Textile Multiband Antenna for WBAN Applications," *IEEE Transactions on Antennas and Propagation*, vol. 71, no. 2, pp. 1391–1402, 2023.

74. Jiang, Z. H., Z. Cui, T. Yue, Y. Zhu and D. H. Werner, "Compact, Highly Efficient, and Fully Flexible Circularly Polarized Antenna Enabled by Silver Nanowires for Wireless Body-area Networks," *IEEE Transactions on Biomedical Circuits and Systems*, vol. 11, no. 4, pp. 920–932, 2017.

75. Low, J.-H., P.-S. Chee and E.-H. Lim, "Liquid EBG-backed Stretchable Slot Antenna for Human Body," *IEEE Transactions on Antennas and Propagation*, vol. 70, no. 10, pp. 9120–9129, 2022.

76. Yang, F. *et al.*, "Strain-invariant Stretchable Antennas via Radical Surface Current Redistributions: Theory, Design, and Experiments," *IEEE Transactions on Antennas and Propagation*, vol. 73, no. 8, pp. 5278–5290, 2025.

77. Hamouda, Z., J.-L. Wojkiewicz, A. A. Pud, L. Koné, S. Bergheul and T. Lasri, "Magnetodielectric Nanocomposite Polymer-based Dual-band Flexible Antenna for Wearable Applications," *IEEE Transactions on Antennas and Propagation*, vol. 66, no. 7, pp. 3271–3277, 2018.

78. Catarinucci, L., F. P. Chietera and R. Colella, "Permittivity-customizable Ceramic-doped Silicone Substrates Shaped with 3D-printed Molds to Design Flexible and Conformal Antennas," *IEEE Transactions on Antennas and Propagation*, vol. 68, no. 6, pp. 4967–4972, 2020.

79. Yin, X., T. Stuart, S. J. Chen, M. Farley, P. Gutruf and C. Fumeaux, "Biosymbiotic 3D-printed Planar Inverted-F Antenna," *IEEE Transactions on Antennas and Propagation*, vol. 72, no. 1, pp. 412–423, 2024.

80. Ramadan, M. and R. Dahle, "Characterization of 3D Printed Flexible Heterogeneous Substrate Designs for Wearable Antennas," *IEEE Transactions on Antennas and Propagation*, vol. 67, no. 5, pp. 2896–2903, 2019.

81. Sayem, A. S. M., R. B. V. B. Simorangkir, K. P. Esselle and R. M. Hashmi, "Development of Robust Transparent Conformal Antennas Based on Conductive Mesh–Polymer Composite for Unobtrusive Wearable Applications," *IEEE Transactions on Antennas and Propagation*, vol. 67, no. 12, pp. 7216–7224, 2019.

82. Samal, P. B., S. J. Chen and C. Fumeaux, "Flexible Hybrid-substrate Dual-band Dual-mode Wearable Antenna," *IEEE Transactions on Antennas and Propagation*, vol. 72, no. 2, pp. 1286–1296, 2024.

83. Casula, G. A. *et al.*, "Design of On-body Epidermal Antenna on AMC Substrate for UHF RFID in Healthcare," *IEEE Transactions on Antennas and Propagation*, vol. 72, no. 5, pp. 4023–4035, 2024.

84. Amendola, S., A. Palombi and G. Marrocco, "Inkjet Printing of Epidermal RFID Antennas by Self-sintering Conductive Ink," *IEEE Transactions on Microwave Theory and Techniques*, vol. 66, no. 3, pp. 1561–1569, 2018.

85. Xu, H. *et al.*, "Flexible Gas-permeable and Resilient Bowtie Antenna for Tensile Strain and Temperature Sensing," *IEEE Internet of Things Journal*, vol. 9, no. 22, pp. 23215–23223, 2022.

86. Lin, X., Y. Chen, Z. Gong, B.-C. Seet, L. Huang and Y. Lu, "Ultrawideband Textile Antenna for Wearable Microwave Medical Imaging Applications," *IEEE Transactions on Antennas and Propagation*, vol. 68, no. 6, pp. 4238–4249, 2020.

87. Sultan, K. S. and A. M. Abbosh, "Wearable Dual Polarized Electromagnetic Knee Imaging System," *IEEE Transactions on Biomedical Circuits and Systems*, vol. 16, no. 2, pp. 296–311, 2022.

88. Sultan, K. S., A. Mahmoud and A. M. Abbosh, "Textile Electromagnetic Brace for Knee Imaging," *IEEE Transactions on Biomedical Circuits and Systems*, vol. 15, no. 3, pp. 522–536, 2021.

89. Saied, I. M. and T. Arslan, "Noninvasive Wearable RF Device Toward Monitoring Brain Atrophy and Lateral Ventricle Enlargement," *IEEE Journal of Electromagnetics, RF and Microwaves in Medicine and Biology*, vol. 4, no. 1, pp. 61–68, 2020.

90. Bahramiabarghouei, H., E. Porter, A. Santorelli, B. Gosselin, M. Popović and L. A. Rusch, "Flexible 16 Antenna Array for Microwave Breast Cancer Detection," *IEEE Transactions on Biomedical Engineering*, vol. 62, no. 10, pp. 2516–2525, 2015.

91. Alqadami, A. S. M., A. E. Stancombe, K. S. Bialkowski and A. Abbosh, "Flexible Meander-line Antenna Array for Wearable Electromagnetic Head Imaging," *IEEE Transactions on Antennas and Propagation*, vol. 69, no. 7, pp. 4206–4211, 2021.

92. Alqadami, A. S. M., B. Mohammed, K. S. Bialkowski and A. Abbosh, "Fabrication and Characterization of Flexible Polymer Iron Oxide Composite Substrate for the Imaging Antennas of Wearable Head Imaging Systems," *IEEE Antennas and Wireless Propagation Letters*, vol. 17, no. 8, pp. 1364–1368, 2018.

93. Alqadami, A. S. M., A. Zamani, A. Trakic and A. Abbosh, "Flexible Electromagnetic Cap for Three-dimensional Electromagnetic Head Imaging," *IEEE Transactions on Biomedical Engineering*, vol. 68, no. 9, pp. 2880–2891, 2021.

94. Alqadami, A. S. M., A. Trakic, A. E. Stancombe, B. Mohammed, K. Bialkowski and A. Abbosh, "Flexible Electromagnetic Cap for Head Imaging," *IEEE Transactions on Biomedical Circuits and Systems*, vol. 14, no. 5, pp. 1097–1107, 2020.

95. Chen, H. *et al.*, "Asymmetrical Planar Folded Dipole Antennas for Human Body MRI at 7 T," *IEEE Transactions on Antennas and Propagation*, vol. 73, no. 5, pp. 2766–2779, 2025.

96. Zhang, H. *et al.*, "Study on Microwave Thorax Imaging for Human Respiration Monitoring," *IEEE Journal of Electromagnetics, RF and Microwaves in Medicine and Biology*, vol. 8, no. 2, pp. 190–197, 2024.

97. Singh, A. *et al.*, "Microwave Antenna-assisted Machine Learning: A Paradigm Shift in Non-invasive Brain Hemorrhage Detection," *IEEE Access*, vol. 12, pp. 37179–37191, 2024.

98. Gong, Z., Y. Ding, Y. Chen and M. J. Cree, "Wearable Microwave Medical Sensing for Stroke Classification and Localization: A Space-division-based Decision-tree Learning Method," *IEEE Transactions on Antennas and Propagation*, vol. 71, no. 8, pp. 6906–6917, 2023.

99. Rezaeieh, S. A. *et al.*, "Wearable Electromagnetic Belt for Steatotic Liver Detection Using Multivariate Energy Statistics," *IEEE Access*, vol. 8, pp. 201847–201860, 2020.

100. Zhang, H. *et al.*, "A Low-profile Compact Dual-band L-shape Monopole Antenna for Microwave Thorax Monitoring," *IEEE Antennas and Wireless Propagation Letters*, vol. 19, no. 3, pp. 448–452, 2020.

101. Buxi, D. *et al.*, "Systolic Time Interval Estimation Using Continuous Wave Radar with On-body Antennas," *IEEE Journal of Biomedical and Health Informatics*, vol. 22, no. 1, pp. 129–139, 2018.

102. Agrawal, D. R. *et al.*, "Conformal Phased Surfaces for Wireless Powering of Bioelectronic Microdevices," *Nature Biomedical Engineering*, vol. 1, no. 3, Art. no. 0043, 2017.

103. Zulkefli, M. S. *et al.*, "Experimental Wireless Link and SAR Assessments of an Implantable PIFA for Biotelemetry in the 2.45 GHz Band," *IEEE Journal of Electromagnetics, RF and Microwaves in Medicine and Biology*, vol. 7, no. 3, pp. 281–289, 2023.

104. Ramli, M. N. *et al.*, "Flexible Dual-band AMC-backed PDMS Antenna with Fluidic Metal for WBAN and WLAN," *12th European Conference on Antennas and Propagation*, London, U.K., pp. 1–3, 2018.

105. Zhang, K., M. Särestöniemi, S. Myllymäki, P. J. Soh, J. Chen and S. Yan, "A Wideband Circularly Polarized Antenna with Metasurface Plane for Biomedical Telemetry," *IEEE Antennas and Wireless Propagation Letters*, vol. 23, no. 6, pp. 1879–1883, 2024.

106. Tian, X., Q. Zeng, D. T. Nguyen and J. S. Ho, "Textile-integrated Phased Surfaces for Wireless Networking of Bioelectronic Devices," *IEEE Transactions on Antennas and Propagation*, vol. 72, no. 1, pp. 267–276, 2024.

107. Tian, X. *et al.*, "Implant-to-implant Wireless Networking with Metamaterial Textiles," *Nature Communications*, vol. 14, no. 1, Art. no. 4335, 2023.

108. Pham, V. L., S. Xuat Ta and H. Yoo, "Wearable Metamaterial Textile for Enhanced Spatial Coverage of Deeply Implanted Device Communication System," *IEEE Transactions on Antennas and Propagation*, vol. 73, no. 7, pp. 4804–4813, 2025.

109. Hasni, U., M. E. Piper, J. Lundquist and E. Topsakal, "Screen-printed Fabric Antennas for Wearable Applications," *IEEE Open Journal of Antennas and Propagation*, vol. 2, pp. 591–598, 2021.

110. Zada, M., I. A. Shah, A. Basir and H. Yoo, "IoMT-enabled Smart-cap-powered Ultrawideband Brain Implant for Multichannel Epilepsy Monitoring Applications,"

IEEE Internet of Things Journal, vol. 12, no. 11, pp. 17051–17065, 2025.

111. Ahmad, A. and D.-Y. Choi, "Efficient Metamaterial-integrated Radiative Near-field Wireless Power Transfer System for Scalp-implantable Devices in IoMT Applications," *IEEE Internet of Things Journal*, vol. 12, no. 13, pp. 25879–25891, 2025.

112. Shah, I. A., M. Zada, S. A. A. Shah, A. Basir and H. Yoo, "Flexible Metasurface-coupled Efficient Wireless Power Transfer System for Implantable Devices," *IEEE Transactions on Microwave Theory and Techniques*, vol. 72, no. 4, pp. 2534–2547, 2024.

113. Koutsoupidou, M., D. C. Tzarouchis, D. Rompolas, I. Sotiriou, G. Palikaras and P. Kosmas, "Wearable Pad for Enhancing EM Coupling with Biological Tissues," *IEEE Transactions on Antennas and Propagation*, vol. 73, no. 3, pp. 1725–1731, 2025.

114. Asif, S. M., A. Iftikhar, J. W. Hansen, M. S. Khan, D. L. Ewert and B. D. Braaten, "A Novel RF-powered Wireless Pacing via a Rectenna-based Pacemaker and a Wearable Transmit-antenna Array," *IEEE Access*, vol. 7, pp. 1139–1148, 2019.

115. Sarestoniemi, M., M. Sonkki, S. Myllymaki and C. Pomalaza-Raez, "Wearable Flexible Antenna for UWB On-body and Implant Communications," *Telecom*, vol. 2, no. 3, pp. 285–301, 2021.

116. Khaleghi, A., A. Hasanvand and I. Balasingham, "Radio Frequency Backscatter Communication for High Data Rate Deep Implants," *IEEE Transactions on Microwave Theory and Techniques*, vol. 67, no. 3, pp. 1093–1106, 2019.

117. Gao, R., H. Sun, R. Ren and H. Zhang, "Design of a Biomedical Antenna System for Wireless Communication of Ingestible Capsule Endoscope," *IEEE Antennas and Wireless Propagation Letters*, vol. 23, no. 12, pp. 4243–4247, 2024.

118. Kiourti, A., J. R. Costa, C. A. Fernandes and K. S. Nikita, "A Broadband Im-

plantable and a Dual-band On-body Repeater Antenna: Design and Transmission Performance," *IEEE Transactions on Antennas and Propagation*, vol. 62, no. 6, pp. 2899–2908, 2014.

119. Godeneli, K., U. Bengi, O. A. Kati and S. Dumanli, "A Wearable Dual-mode Repeater Antenna for Implant Communications," *IEEE Transactions on Antennas and Propagation*, vol. 70, no. 2, pp. 868–875, 2022.

120. Magill, M. K., G. A. Conway and W. G. Scanlon, "Circularly Polarized Dual-mode Wearable Implant Repeater Antenna with Enhanced Into-body Gain," *IEEE Transactions on Antennas and Propagation*, vol. 68, no. 5, pp. 3515–3524, 2020.

121. Agneessens, S., P. Van Torre, E. Tanghe, G. Vermeeren, W. Joseph and H. Rogier, "On-body Wearable Repeater as a Data Link Relay for In-body Wireless Implants," *IEEE Antennas and Wireless Propagation Letters*, vol. 11, pp. 1714–1717, 2012.

122. Blauert, J. and A. Kiourti, "Theoretical Modeling and Design Guidelines for a New Class of Wearable Bio-matched Antennas," *IEEE Transactions on Antennas and Propagation*, vol. 68, no. 3, pp. 2040–2049, 2020.

123. Blauert, J. and A. Kiourti, "Bio-matched Horn: A Novel 1–9 GHz On-body Antenna for Low-loss Biomedical Telemetry with Implants," *IEEE Transactions on Antennas and Propagation*, vol. 67, no. 8, pp. 5054–5062, 2019.

124. Blauert, J. and A. Kiourti, "Bio-matched Antennas with Flare Extensions for Reduced Low Frequency Cutoff," *IEEE Open Journal of Antennas and Propagation*, vol. 1, pp. 136–141, 2020.

125. Rice, A. and A. Kiourti, "High-contrast Low-loss Antenna: A Novel Antenna for Efficient Into-body Radiation," *IEEE Transactions on Antennas and Propagation*, vol. 70, no. 11, pp. 10132–10140, 2022.

126. Miah, M. S., A. N. Khan, C. Icheln, K. Haneda and K.-I. Takizawa, "Antenna

System Design for Improved Wireless Capsule Endoscope Links at 433 MHz," *IEEE Transactions on Antennas and Propagation*, vol. 67, no. 4, pp. 2687–2699, 2019.

127. Perez-Simbor, S., C. Andreu, C. Garcia-Pardo, M. Frasson and N. Cardona, "UWB Path Loss Models for Ingestible Devices," *IEEE Transactions on Antennas and Propagation*, vol. 67, no. 8, pp. 5025–5034, 2019.

128. Liu, H. *et al.*, "Novel Multiband Antenna Design and Performance Evaluation for Wireless Electronic Capsule Systems," *IEEE Journal of Electromagnetics, RF and Microwaves in Medicine and Biology*, vol. 8, no. 4, pp. 332–343, 2024.

129. Iqbal, A., A. Smida, M. Al-Hasan, I. Ben Mabrouk and T. A. Denidni, "Highly Isolated Wireless Power Transfer and Information Co-delivery Using a Pacemaker Duplex Antenna," *IEEE Transactions on Microwave Theory and Techniques*, vol. 73, no. 2, pp. 1158–1170, 2025.

130. Zhang, K. *et al.*, "Near-field Wireless Power Transfer to Deep-tissue Implants for Biomedical Applications," *IEEE Transactions on Antennas and Propagation*, vol. 68, no. 2, pp. 1098–1106, 2020.

131. Fang, X., X. Du, M. Bärhold, Q. Wang and D. Plettemeier, "MICS-band Helical Dipole Antenna for Biomedical Implants," *IEEE Antennas and Wireless Propagation Letters*, vol. 21, no. 12, pp. 2502–2506, 2022.

132. Gutierrez-Hernandez, M., S. P. Duarte, D. P. Triana, S. Bojja-Venkatakrishnan, J. R. Diaz and J. L. Volakis, "Lightweight, Battery-less and Wireless Sensor for Monitoring Neuronal Activity in Swine," *IEEE Journal of Electromagnetics, RF and Microwaves in Medicine and Biology*, pp. 1-9, 2025.

133. Lamkaddem, A., A. El Yousfi, Y. Huang, V. González Posadas and D. Segovia-Vargas, "Miniaturized Wireless Power Transfer System with a Dual-band Implantable Antenna for Multifunctional Biomedical Devices," *IEEE Sensors Journal*,

vol. 25, no. 16, pp. 31473–31488, 2025.

134. Rashid, S. *et al.*, "3D Printed UWB Microwave Bodyscope for Biomedical Measurements," *IEEE Antennas and Wireless Propagation Letters*, vol. 18, no. 4, pp. 626–630, 2019.

135. Mouzi, V., N. Moraitis, C. Kakoyiannis, K. S. Nikita and C. Valagiannopoulos, "Efficient Power Transfer to Implanted Antennas," *IEEE Access*, vol. 13, pp. 119884–119896, 2025.

136. Cadir, C., O. A. Kati and S. Dumanli, "Matching Medium Design for In-body Communications Using Artificial Neural Networks," *15th European Conference on Antennas and Propagation (EuCAP)*, Dusseldorf, Germany, pp. 1-5, 2021.

137. Paul, S., N. K. Tiwari and M. J. Akhtar, "Design of Highly Directive GRIN MS Lens Integrated DFHA for Deep Tissue Biomedical Imaging," *IEEE Transactions on Antennas and Propagation*, vol. 71, no. 1, pp. 330–341, 2023.

138. Brizi, D., M. Conte and A. Monorchio, "A Performance-enhanced Antenna for Microwave Biomedical Applications by Using Metasurfaces," *IEEE Transactions on Antennas and Propagation*, vol. 71, no. 4, pp. 3314–3323, 2023.

139. Wang, H., L. Zhu, Y. Feng and Y.-X. Guo, "Design of a Compact Dual-polarized Wearable Antenna with Spatial Diversity Reception for Into-body Communications," *IEEE Transactions on Antennas and Propagation*, vol. 71, no. 10, pp. 7911–7923, 2023.

140. Wang, H., Y. Feng, F. Hu and Y.-X. Guo, "A Wideband Dual-polarized Ring-loaded Cross Bowtie Antenna for Wireless Capsule Endoscopes: Design and Link Analysis," *IEEE Transactions on Antennas and Propagation*, vol. 70, no. 9, pp. 7843–7852, 2022.

141. Noormohammadi, R., A. Khaleghi, J. Bergsland and I. Balasingham, "Conduc-

tive Backscatter Communication for Dual-chamber Leadless Pacemakers," *IEEE Transactions on Microwave Theory and Techniques*, vol. 70, no. 4, pp. 2442–2450, 2022.

142. Bilir, A. and S. Dumanli, "Wide-band Dual Port Cross Slot Wearable Antenna for In-body Communications," *17th European Conference on Antennas and Propagation (EuCAP)*, Florence, Italy, pp. 1–5, 2023.

143. Sturm-Richter, K. *et al.*, "Unbalanced Fermentation of Glycerol in *E. coli* via Heterologous Production of an Electron Transport Chain and Electrode Interaction in Microbial Electrochemical Cells," *Bioresource Technology*, vol. 186, pp. 89–96, 2015.

144. Thirumurthy, M. A. and A. K. Jones, "*Geobacter* Cytochrome OmcZs Binds Riboflavin: Implications for Extracellular Electron Transfer," *Nanotechnology*, vol. 31, no. 12, p. 124001, 2020.

145. Riemer, J., H. H. Hoepken, H. Czerwinska, S. R. Robinson and R. Dringen, "Colorimetric Ferrozine-based Assay for the Quantitation of Iron in Cultured Cells," *Analytical Biochemistry*, vol. 331, no. 2, pp. 370–375, 2004.

146. Saltepe, B., E. U. Bozkurt, M. A. Gungen, A. E. Cicek and U. O. Seker, "Genetic Circuits Combined with Machine Learning Provides Fast Responding Living Sensors," *Biosensors and Bioelectronics*, vol. 178, p. 113028, 2021.

147. Koksaldi, I. C. *et al.*, "SARS-CoV-2 Detection with De Novo-designed Synthetic Riboregulators," *Analytical Chemistry*, vol. 93, no. 28, pp. 9719–9727, 2021.

148. Akboga, D., B. Saltepe, E. U. Bozkurt and U. O. Seker, "A Recombinase-based Genetic Circuit for Heavy Metal Monitoring," *Biosensors*, vol. 12, no. 2, p. 122, 2022.

149. Ahan, R. E., B. M. Kirpat, B. Saltepe and U. O. Seker, "A Self-actuated Cellular

Protein Delivery Machine," *ACS Synthetic Biology*, vol. 8, no. 4, pp. 686–696, 2019.

150. Koksaldi, I. C. *et al.*, "RNA-based Sensor Systems for Affordable Diagnostics in the Age of Pandemics," *ACS Synthetic Biology*, vol. 13, no. 4, pp. 1026–1037, 2024.

151. Saltepe, B., E. U. Bozkurt, N. Hacıosmanoğlu and U. Ö. Şeker, "Genetic Circuits to Detect Nanomaterial Triggered Toxicity Through Engineered Heat Shock Response Mechanism," *ACS Synthetic Biology*, vol. 8, no. 10, pp. 2404–2417, 2019.

152. Kuster, N. *et al.*, "Tissue Properties Database," IT'IS Foundation, Zurich, Switzerland. [Online]. Available: https://itis.swiss/database, Accessed on September 15, 2025.

153. Xiong, L. L. *et al.*, "Tunable Temperature-sensitive Transcriptional Activation Based on Lambda Repressor," *ACS Synthetic Biology*, vol. 11, no. 7, pp. 2518–2522, 2022.

154. Saltepe, B. *et al.*, "Genetic Circuits to Detect Nanomaterial Triggered Toxicity Through Engineered Heat Shock Response Mechanism," *ACS Synthetic Biology*, vol. 8, no. 10, pp. 2404–2417, 2019.

155. Piraner, D. I. *et al.*, "Tunable Thermal Bioswitches for In Vivo Control of Microbial Therapeutics," *Nature Chemical Biology*, vol. 13, no. 1, pp. 75–80, 2016.

156. Ping, A. *et al.*, "Targeted Optical Neural Stimulation: A New Era for Personalized Medicine," *Frontiers in Neuroscience*, vol. 29, no. 2, pp. 202–220, 2021.

157. ANSYS Inc., "ANSYS HFSS, High Frequency Structure Simulator," version 2023 R2, Canonsburg, PA, USA.

158. Soares, I. V., M. Gao, E. Cil, Z. Šipuš, A. K. Skrivervik, J. S. Ho and D. Nikolayev, "Wireless Powering Efficiency of Deep-body Implantable Devices," *IEEE Transactions on Microwave Theory and Techniques*, vol. 71, no. 6, pp. 2680–2692, 2022.

159. Dumanli, S., "Challenges of Wearable Antenna Design," in *46th European Microwave Conference (EuMC)*, London, U.K., pp. 1350–1352, 2016.

APPENDIX A: LIST OF PUBLICATIONS

The publications related to this thesis are listed below.

1- **A. Bilir**, M. Yavuz, U.O.S. Seker, and S. Dumanli, "Wireless In-body Sensing through Genetically Engineered Bacteria," *Nature Communications*, accepted.

2- C. Karabulut, **A. Bilir**, M. E. Lacin and S. Dumanli, "3D-Engineered Muscle Tissue as a Wireless Sensor: AntennAlive [Bioelectromagnetics]," in *IEEE Antennas and Propagation Magazine*, vol. 65, no. 6, pp. 28-36, Dec. 2023.

3- O. F. Sezgen, O. Altan, **A. Bilir**, M. G. Durmaz, N. Haciosmanoglu, B. Camli, Z. C. Canbek Ozdil, A. E. Pusane, A. D. Yalcinkaya, U. O. S. Seker, T. Tugcu, and S. Dumanli, "A Multiscale Communications System Based on Engineered Bacteria," in *IEEE Communications Magazine*, vol. 59, no. 5, pp. 62-67, May 2021.

4- I. H. Kacar, **A. Bilir**, U. O. S. Seker, and S. Dumanli, "Wireless Control of Bacterial Function with Microwave Hyperthermia," *2025 IEEE 36th International Symposium on Personal, Indoor and Mobile Radio Communications (PIMRC)*, Istanbul, Turkey, 2025.

5- **A. Bilir** and S. Dumanli, "Biodegradable Implant Antenna Utilized for Real-Time Sensing through Genetically Modified Bacteria," *2024 18th European Conference on Antennas and Propagation (EuCAP)*, Glasgow, United Kingdom, 2024, pp. 1-4.

6- **A. Bilir** and S. Dumanli, "Temperature-Dependent Electrical Characterization of a Thermally Sensitive Hepatic Tumor Phantom," *2024 18th European Conference on Antennas and Propagation (EuCAP)*, Glasgow, United Kingdom, 2024, pp. 1-5.

7- **A. Bilir** and S. Dumanli, "Wide-band Dual Port Cross Slot Wearable Antenna for In-body Communications", *2023 17th European Conference on Antennas and Propagation (EuCAP)*, Florence, Italy, 2023, pp. 1-5.

8- O. K. Erden, **A. Bilir**, C. Karabulut, U. O. S. Seker, and S. Dumanli, "An-

tennas Reconfigured by Living Cells: AntennAlive", *IEEE International Symposium on Antennas and Propagation and USNC-URSI Radio Science Meeting (AP-S/URSI)*, 2022, pp. 882-883.

APPENDIX B: COPYRIGHT AND REUSE PERMISSION STATEMENT

The figures created within the scope of this thesis and whose copyrights have been transferred to the publisher have been used in this thesis book in accordance with the publisher's policy on "reuse of author-generated text and graphics," as stated on the publisher's official website. These figures originate from the following publications:

- A. Bilir, M. Yavuz, U.O.S. Seker, and S. Dumanli, "Wireless In-body Sensing through Genetically Engineered Bacteria," *Nature Communications*, accepted.
- I. H. Kacar, A. Bilir, U.O.S. Seker, and S. Dumanli, "Wireless Control of Bacterial Function with Microwave Hyperthermia," *2025 IEEE 36th International Symposium on Personal, Indoor and Mobile Radio Communications (PIMRC)*, Istanbul, Turkey, 2025.